

Algorithm Theoretical
Basis Document For
Cloud Top Temperature
and Pressure

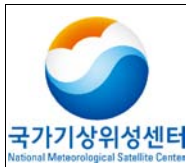
Code:NMSC/SCI/ATBD/CTTP
Issue:1.0 Date:2012.12.26
File: CTTP-ATBD_V5.0.hwp
Page : 1/40



CTTP Algorithm Theoretical Basis Document

NMSC/SCI/ATBD/CTTP, Issue 1, rev.5

26 December 2012

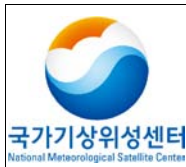


Algorithm Theoretical
Basis Document For
Cloud Top Temperature
and Pressure

Code:NMSC/SCI/ATBD/CTTP
Issue:1.0 Date:2012.12.26
File: CTPP-ATBD_V5.0.hwp
Page : 1/40

REPORT SIGNATURE TABLE

Function	Name	Signature	Date
Prepared by	Yong-Sang Choi, Heaje Cho		26 December 2012
Reviewed by	Yong-Sang Choi		26 December 2012
Authorised by	NMSC		26 December 2012

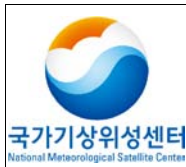


Algorithm Theoretical
Basis Document For
Cloud Top Temperature
and Pressure

Code:NMSC/SCI/ATBD/CTTP
Issue:1.0 Date:2012.12.26
File: CTTP-ATBD_V5.0.hwp
Page : 1/40

DOCUMENT CHANGE RECORD

Version	Date	Pages	Changes
Version5	26 December 2012	5 page	- The method defined brightness temperature of clear pixel change. - In the previous defined the clear pixel compared with brightness temperature of the neighboring pixel, but changed to use the maximum value of brightness temperature between 15 days.
Version5	26 December 2012	19 page	- Add improvement of underestimated cloud top temperature
Version5	26 December 2012	20 Page	- Insert regression coefficient table of re-retrieved optimal corresponding cloud top temperature - Add modified result in Fig 11.

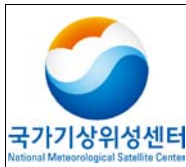


Algorithm Theoretical
Basis Document For
Cloud Top Temperature
and Pressure

Code:NMSC/SCI/ATBD/CTTP
Issue:1.0 Date:2012.12.26
File: CTTP-ATBD_V5.0.hwp
Page : 1/40

Table of Contents

1. Overview
2. Background and purpose
3. Algorithm
 - 3.1 Theoretical background and basis
 - 3.2 Retrieval method
 - 3.2.1 Single channel method
 - 3.2.2 Radiation ratio method
 - 3.3 Retrieval process
 - 3.3.1 Input data
 - 3.3.2 Pre-processing Process
 - 3.3.3 Algorithm
 - 3.3.4 QC flag
 - 3.4 Validation
 - 3.4.1 Validation method
 - 3.4.2 Validation data
 - 3.4.3 Temporal and spatial collocation method
 - 3.4.4 Validation result analysis
4. Interpretation of retrieval results
5. COMS version and algorithm improvement after COMS satellite launch
6. Problems and possibilities for improvement
7. References



Algorithm Theoretical
Basis Document For
Cloud Top Temperature
and Pressure

Code:NMSC/SCI/ATBD/CTTP
Issue:1.0 Date:2012.12.26
File: CTP-ATBD_V5.0.hwp
Page : 1/40

List of Tables

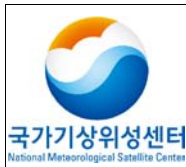
Table 1 : QC flag.

Table 2 : Definitions of terms used in this analysis.

Table 3 : Validation results of CTP

Table 4 : Detailed Output data for the CTP algorithm.

Table 5 : Modification of lookup table for CMDPS CTP



Algorithm Theoretical
Basis Document For
Cloud Top Temperature
and Pressure

Code:NMSC/SCI/ATBD/CTTP
Issue:1.0 Date:2012.12.26
File: CTTP-ATBD_V5.0.hwp
Page : 1/40

List of Figures

Figure 1 : Climatological atmospheric absorption used to compute cloud top temperature from IR10.8 μm brightness temperature (SAFNWC/MSG user manual, 2002).

Figure 2 : Flow chart of the CTP algorithm.

Figure 3 : JAMI/MTSAT-1R radiance imagery for the five spectral channels centered at 0.725 (VIS), 10.8 (IR1), 12.0 (IR2), 6.75 (IR3), and 3.75 μm (IR4) for 0333 UTC August 7, 2006. Except for the VIS channel, the brighter color corresponds to a relatively low value in $\text{W m}^{-2} \text{sr}^{-1} \text{m}^{-1}$. The full-disk imagery covers East Asia, West Pacific, Australia, and a part of the Antarctic region (80.5S80.5N, 60.4E139.4W).

Figure 4 : Cloud top pressure derived by the CLA from the JAMI level-1b calibrated radiances shown in Figure 3. Base products (left) are the results of conventional methods or without correction methods, and final products (right) from improved methods or with the correction methods developed in the present study.

Figure 5 : Relative frequency distribution (in %) of MODIS CTP (a), base CTP retrieved by the IR1 estimate only (b), and final CTP corrected by the radiance ratioing method (c) for the total clouds. The results are shown for August 2006, daytime, nighttime, Northern and Southern Hemispheres, and the polar, tropical, and midlatitude regions.

Figure 6 : The difference between MTSAT-1R (both base and final) CTP and MODIS CTP values (in %) shown in figure 5. The radiance ratios are calculated by using clear-sky radiances obtained within various spatial resolutions: 12 (3×3), 60 (15×15), 100 (25×25), and 220 km (55×55 pixels).

Figure 7 : Time series of the ratio of ice clouds to the total clouds at nine selected sites; base CTP (a), and final CTP (b).

Figure 8 : Relative frequency of MTSAT minus MODIS CTP (a) for the maximum values. Errors in the retrieved CTP (b) (in %) with respect to the corresponding parameters. The solid and dotted lines indicate values from the final (corrected) and base (uncorrected) products, respectively.


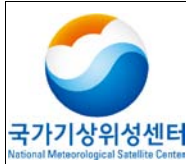
 <p>국가기상위성센터 National Meteorological Satellite Center</p>	<p>Algorithm Theoretical Basis Document For Cloud Top Temperature and Pressure</p>	<p>Code:NMSC/SCI/ATBD/CTTP Issue:1.0 Date:2012.12.26 File: CTPP-ATBD_V5.0.hwp Page : 1/40</p>
--	--	---

Figure 9 : Simulation for radiance ratio and single layer ice-clouds.

Figure 10 : Cloud top pressure (a)before and (b)after correcting discontinuities at $\pm 30^\circ$ latitude.

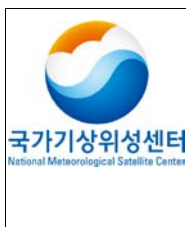


Algorithm Theoretical
Basis Document For
Cloud Top Temperature
and Pressure

Code:NMSC/SCI/ATBD/CTTP
Issue:1.0 Date:2012.12.26
File: CTP-ATBD_V5.0.hwp
Page : 1/40

List of Acronyms

COMS	Communication, Ocean, and Meteorological Satellite
MTSAT	Multi-functional Transport Satellite
JAMI	Japanese Advanced Meteorological Imager
ISCCP	International Satellite Cloud Climatology Project
FOV	Field of view
MODIS	Moderate Resolution Imaging Spectroradiometer
CTT	Cloud Top Temperature
CTP	Cloud Top Pressure
CTH	Cloud Top Height
CTTP	Cloud Top Temperature and Pressure
SBDART	Santa Barbara DISORT Atmospheric Radiative Transfer



Algorithm Theoretical Basis Document For Cloud Top Temperature and Pressure

Code:NMSC/SCI/ATBD/CTTP
Issue:1.0 Date:2012.12.26
File: CTTT-ATBD_V5.0.hwp
Page : 1/40

1. Overview

Cloud Top Temperature and Pressure (CTTP) retrieval algorithm is information that is usefully utilized in various fields such as very short range forecasting support, and Atmospheric Motion Vector (AMV) retrieval. CTTT is a part of information retrieved in the scene analysis. It is produced using cloud detection information and brightness temperature observed from satellite, and results of Radiative Transfer Model (RTM).

Section 2 of this document presents background and the purpose of the CTTT retrieval algorithm. Section 3 explains the algorithm. Section 4 describes the analysis method of retrieval results. Section 5 discusses with problems with the algorithm and possibilities for improvement.

2. Background and purpose

The results of the CTTT algorithm are cloud top temperature, cloud top pressure and cloud top height. The algorithm performs the single channel and radiation ratio method at the same time. The single channel method derives cloud top temperature(K) using $10.8\mu\text{m}$ brightness temperature. It is converted into cloud top pressure (hPa) using atmospheric profile data. If the Numerical Weather Prediction (NWP) model or observation value is not available, we uses climate data prepared in advance.

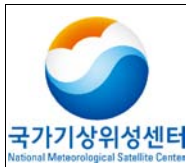
The radiation ratio method derives cloud top pressure using $6.75\mu\text{m}$ and $10.8\mu\text{m}$ channels. This will be used to complement cloud top pressure of semi-transparent clouds. It selects the optimal cloud top pressure by comparing cloud top pressure calculated through two methods. It retrieves cloud top height using a height formula from the selected cloud top pressure.

Cloud top height and temperature can utilize basic data to produce an early diagnosis and alert of thunderstorm development. In other applications, it can support activity in aviation forecasting and can be used as input data for mesoscale models. Also, it is used as input data for classification of ISCCP cloud type. The detailed background purpose for the CTTT algorithm is introduced in detail in the Appendix (Choi et al., 2007).

3. Algorithm

3.1 Theoretical background and basis

The retrieval methods of the CTTT algorithm will find the cloud top pressure through the single



Algorithm Theoretical Basis Document For Cloud Top Temperature and Pressure

Code:NMSC/SCI/ATBD/CTTP
Issue:1.0 Date:2012.12.26
File: CTTP-ATBD_V5.0.hwp
Page : 1/40

channel and radiation ratio methods. The retrieval method is introduced later in this paper. More detailed theory and the basis is described on pages 4,725-4,730 of the Appendix (Choi et al., 2007).

3.2 Retrieval method

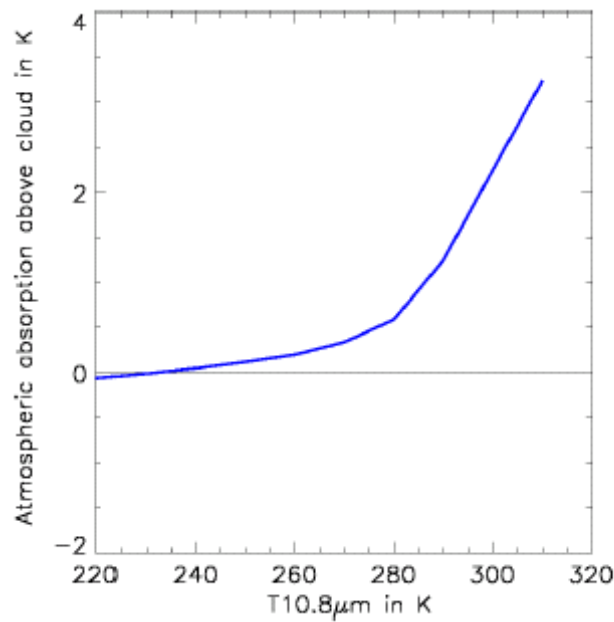
3.2.1 Single channel method

Cloud top temperature is retrieved using an offset value for IR10.8 μm brightness temperature depending on satellite zenith angle. The offset value has a big value when low clouds are present, or the satellite viewing angle is large. The table of offset values are calculated in advance as input data to a brightness temperature of IR10.8 μm (i.e. indicating the height of opaque clouds) and satellite zenith angle.

In the case of calculation, simulation of radiative transfer models is performed offline. Cloud top pressure, and radiative transfer models have to be supported online with atmospheric vertical distribution data. The atmospheric vertical distribution is interpolated as an exact view using the result of the NWP model.

The atmospheric IR10.8 μm brightness temperature is simulated for each different pressure layer by atmospheric vertical distribution data. A suitable cloud top pressure is retrieved as the best fit between the observed IR10.8 μm radiance and the simulated radiance. In the case of a low level inversion layer, if the temperature of a cloud is cooler than the low inversion layer, clouds are regarded as located above the inversion layer.

Fig. 1. Climatological atmospheric absorption used to compute cloud top temperature from IR10.8 μm brightness temperature (SAFNWC/MSG user manual, 2002).



3.2.2. Radiation ratio method

The radiation ratio method is retrieved using two IR channels with cloud top pressure of semi-transparent clouds. Also, RTM simulation data has to be supported online and the atmospheric vertical distribution data is needed. The fundamental equation of this method is shown in equation 1:

$$\frac{R - R_{clear1}}{D} = \frac{N\epsilon_1 (R_{op1})}{N\epsilon_1 / D} \quad (1)$$

Where R_m is observed radiance, R_{clear} is clear sky radiance, and R_{op} is radiance of the opaque cloud (Simulation value). N is the cloudiness, ϵ is the emissivity of cloud. 1, 2 of both sides indicate each IR window channel and WV6.75 μm . If the ratio of emissivity is approximate to 1, equation (1) is simplified as shown in equation 2:

$$\frac{R_{m1} - R_{clear1}}{D} = \frac{R_{op1}}{D} \quad (2)$$

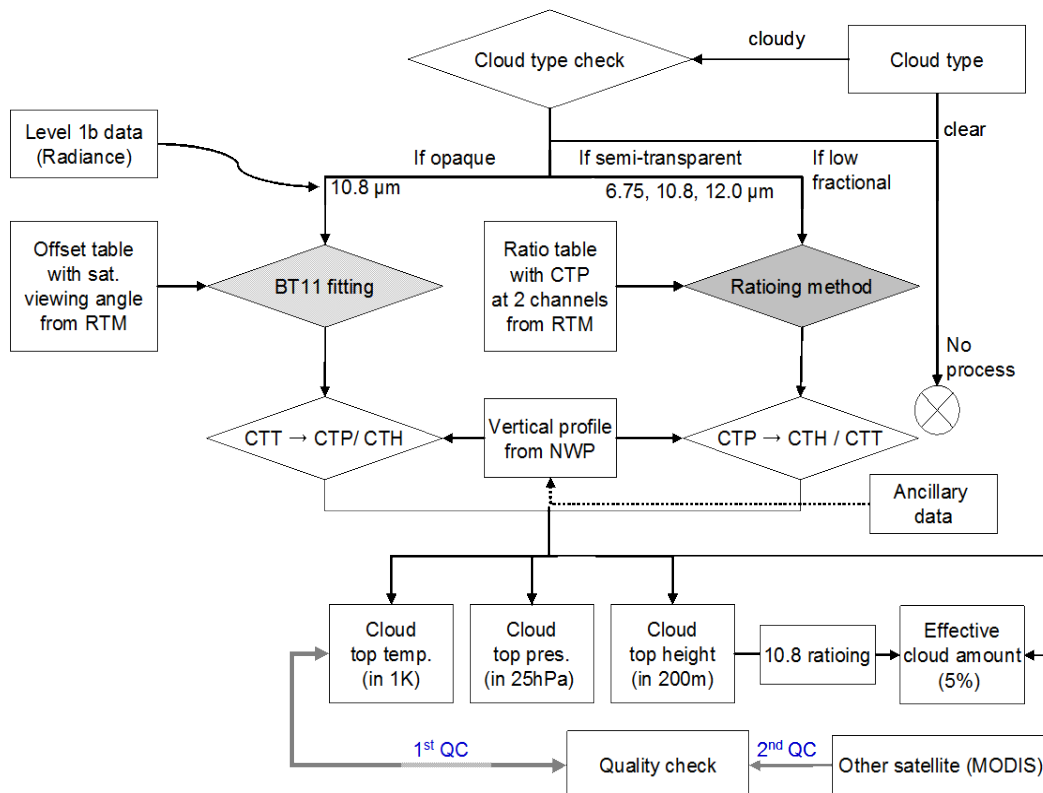
Both sides depend on the selected channel, surface temperature, vertical temperature and absorption distribution. The right side is a value which depends on the cloud top pressure by R_{op} . Consequently, If we use the fixed surface temperature and vertical distribution, the right side becomes a function which depends on the pressure and the left side will become a constant. The retrieved cloud top pressure is the pressure p to satisfy the equation (2).

Radiation ratio method is very sensitive to noise. Especially, it is more sensitive to thin cirrus. Also the simulated radiance in water vapor channel is inaccurate, because the predictability of water vapor is not good. The retrieved cloud top pressure is sent as input data for ISCCP cloud type classification.

3.3 Retrieval process

Fig. 2. is the flowchart of the CTTP retrieval algorithm

Fig. 2. Flow chart of the CTTP algorithm.





Algorithm Theoretical Basis Document For Cloud Top Temperature and Pressure

Code:NMSC/SCI/ATBD/CTTP
Issue:1.0 Date:2012.12.26
File: CTTP-ATBD_V5.0.hwp
Page : 1/40

3.3.1 Input data

The input data of CTPP is divided into static data and dynamic data. Radiance and reflectance, brightness temperature, satellite zenith angle, and scene analysis are derived from Level 1.5 and used as input data. Reflectance has the range of 0~100%, brightness temperature 170~350K, and satellite zenith angle 0~90°. Pre. and Acc, are 0.1. The input data derived in this module include surface temperature, surface pressure, atmospheric temperature and relative humidity of 2m, and temperature and relative humidity on the vertical pressure. Also, the constants of the retrieved values and empirical values have to be prepared in cloud analysis

3.3.2 Pre-processing process

The pre-processing process calculates the value of radiation ratio of IR10.8 μ m and WV μ m depending on the cloud top pressure using “Streamer”/ Radiative Transfer Model. The calculated results for the radiation ratio depend on the tropic, mid-latitude, atmosphere in the polar region showed slightly the difference.

The difference of radiation ratio depends on cloud top pressure in the tropic region strikingly showed, but the value grew less at higher latitudes. We applied the radiation ratio depending on atmospheric profile and latitude to correct this difference.

3.3.3. Algorithm

The most important step of the CTPP algorithm is to find the cloud top pressure by performing the single channel method and radiation ratio method at the same time. The single channel method uses the properties from channel of infrared window IR10.8 μ m, which changes the value depending on the height of the cloud.

Radiation ratio method uses brightness temperatures of IR10.8 μ m and WV6.7 μ m. The single channel method uses cloud top temperature using the simple function from brightness temperature of 10.8 μ m. The coefficient of the function depends on the satellite zenith angle. Cloud top pressure is extracted to compare with the retrieved cloud top temperature in advance and atmosphere profile of NWP. If the semi-transparent cloud is located at high level, brightness temperature of IR10.8 μ m is influenced not only by the cloud but also the surface. The values for cloud top temperature and pressure of high level semi-transparent clouds retrieved by single channel method have errors.

In order to compensate for this problem, the radiation ratio method is used. The radiation ratio method will use the ratio of the difference in brightness temperature between clear sky and cloudy conditions of two channels (WV6.75 μ m and IR10.8 μ m). This equation is expressed as follows:

$$\frac{I_m - I_{cc,m}}{I_n - I_{cc,n}} = \frac{I_{op,m} - I_{cc,m}}{I_{op,n} - I_{cc,n}} = R \quad (3)$$

I_{op,m} and I_{cc,m} mean the radiance of semi-transparent cloud and the brightness temperature of clear sky of each channels m. The equation (3) is applied in the case of semi-transparent clouds on the assumption that the transmittance of the cloud for each channel is the same. The ratio R of the equation (3) is a function of cloud top height. The channel m and n use the brightness temperature of IR10.8 μ m and WV6.7 μ m. Brightness temperatures of clear sky pixel use the maximum value of brightness temperature of a 15-day period in each pixel. We retrieve cloud top pressure to compare with the calculated radiation ratio and results of the radiative transfer model.

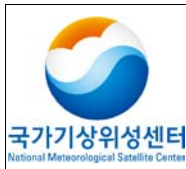
Single channel method and radiation ratio method select the final cloud top pressure which have a low value comparing with the result retrieved using each method. If using the single channel method to retrieve the pressure of semi-transparent clouds, it is retrieved higher than the existing pressure. The retrieved result using the radiation ratio can compensate for the single channel method. The center of WV6.7 μ m weighting function is 400~500 hPa. The radiation ratio method can be applied to high clouds.

This algorithm retrieves cloud top pressure correcting in consequence of radiation ratio for cloud top pressure of semi-transparent clouds in the single channel method. We retrieve cloud top height using the function between pressure and height into this retrieved cloud top pressure.

3.3.4. QC flag

QC flag for cloud top pressure is listed in table 1. QC flag for cloud top pressure in the algorithm, the final selected cloud top pressure presents 128 for single channel method, 64 for radiation ratio method. Finally, if the cloud top pressure is not retrieved, it presents as flag 0.

Table 1. QC flag



**Algorithm Theoretical
Basis Document For
Cloud Top Temperature
and Pressure**

Code:NMSC/SCI/ATBD/CTTP
Issue:1.0 Date:2012.12.26
File: CTTP-ATBD_V5.0.hwp
Page : 1/40

CLA - CTP

bit	Bit Interpretation	Field Description
8(Method in final cloud top pressure)	128	IR window estimate
unavail => 0	64	Radiance rationing method

3.4 Validation

3.4.1 Validation method

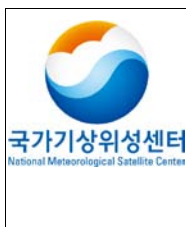
3.4.1.1. Pre-processing process for validation- Simplified ISCCP cloud detection

We used calibrated radiance and brightness temperature of a hourly Full-disk provided from JAMI sensors on board MTSAT as simulated images of COMS as input data. The central wavelength of 5 channel from JAMI are located at $0.725\mu\text{m}$ (VIS), $10.8\mu\text{m}$ (IR1), $12.0\mu\text{m}$ (IR2), $6.75\mu\text{m}$ (IR3), and $3.7\mu\text{m}$ (IR4).

The pre-processing process needs to distinguish clear pixels between clouds and clear in order to validate of cloud information product. In the operation, the cloud detection algorithm played this role in CMDPS algorithm, but this validation of algorithm utilized the simplified International Satellite Cloud Climatology Project (ISCCP) cloud detection technique (Rossow and Garder 1993a). For cloud detection, ISCCP uses the spectral test of VIS and IR channels as follows:

$$\begin{aligned}
 \text{Clear: } & (BT_{IR1}^{clr} - BT_{IR1}) \leq IRTHR \text{ and } (L_{VIS} - L_{VIS}^{clr}) \leq VISTHR \\
 \text{Cloudy: } & (BT_{IR1}^{clr} - BT_{IR1}) > IRTHR \text{ or } (L_{VIS} - L_{VIS}^{clr}) > VISTHR
 \end{aligned} \tag{4}$$

Where, BT_{IR1}^{clr} is brightness temperature of IR1 in all sky, BT_{IR1} is brightness temperature of IR1 in clear sky, L_{VIS} is radiance of VIS in all sky, L_{VIS}^{clr} is radiance of VIS in clear sky. L_{VIS} is the adjusted radiance by the percent ratio, which is the same as the ISCCP algorithm. IRTHR of threshold value is 12.0K, VISTHR is 6.0% for the land, and 3.0 for the ocean. The availability of cloud detection have to consider to determine mainly by the accuracy of the clear sky radiance (Rossow and Garder 1993b). In this validation, BT_{IR1}^{clr} (L_{VIS}^{clr}) set the maximum and minimum value for each UTC in the month of August, 2006.



Algorithm Theoretical Basis Document For Cloud Top Temperature and Pressure

Code:NMSC/SCI/ATBD/CTTP
Issue:1.0 Date:2012.12.26
File: CTTT-ATBD_V5.0.hwp
Page : 1/40

VISTHR is the same as the value of ISCCP, because it is high calculated brightness temperature of IR clear sky. IRTHR is higher 6K for land, 1K for the ocean than the value suggested by Rossow and Gardar (1993a). Therefore, the selection of cloud pixels is stricter than the ISCCP algorithm. We use IR condition of equation (4) during nighttime. The detected cloud amount by the above method accounts for the average CA for August, 2006 about 57.3 % in JAMI Field Of View (FOV). This value is comparable with estimation results of other global CA climate data. Rossow et al. (1993), estimated 62.7% in ISCCP C2 (1984-1988), 61.2% in Gridded surface weather station reports (SOBS) (1971-1981), 61.4% in METEOR (1976-1988), and 51.8% in Nimbus-7 (1980-1984). A notable point is that it has a higher cloud amount than the JAMI cloud amount of MODIS , which was an average of 77.6% during the validation period.

It has 18 bands from MODIS in a narrower Field of View (FOV), because it detects clouds of various shape including thin cirrus. Therefore, the results of cloud detection by this method will contain a considerable uncertainty as compared with reality. This is obvious that have the cloud information product or uncertainty using the result of cloud detection

3.4.1.2. Explanation of validation method

Validation is performed for Full-disk images of JAMI in the month of August, 2006. This period is decided to consider a limited calculation space, but Field of view (FOV) of this period included all situations that have the surface, cloud type, vertical distribution of atmospheric gas, observation and sun zenith angle affecting the detection via geostationary satellite.

Besides, during this period typhoons such as *Saomi* and *Bopha* reached the Korean Peninsula and Japan. When the main purpose of COMS utilization is to predict heavy weather, these validation periods are optimal for examining the performance capacity of the algorithm.

This cloud validation has two types of products. It improves the current version in comparison/validation with “base product” retrieved by traditional algorithm and the “final product“ of the current version algorithm which was independently developed by a team lead by Professor Chang-Hoi Ho at Seoul National University.

Basic cloud top height was retrieved using the radiance from the IR1 channel. Final cloud top height is a value to correct basic cloud top height by radiation ratio method (Choi et al. 2007) between IR1 and IR3 channels. The designations of each product used in this validation are summarized in Table 2.


	Algorithm Theoretical Basis Document For Cloud Top Temperature and Pressure	Code:NMSC/SCI/ATBD/CTTP Issue:1.0 Date:2012.12.26 File: CTPP-ATBD_V5.0.hwp Page : 1/40
---	--	---

Table 2. Definitions of terms used in this analysis.

Term	Unit	Definition
Base CTP	hPa	Cloud top pressure is retrieved by the IR1 window estimate.
Final CTP	hPa	Cloud top pressure is retrieved by both the IR1 window estimate and the radiance ratioing method using IR1 and IR3 radiances.

Above are defined the basic, final, and MODIS products compared with four procedures. It corrects into optimal condition algorithm of four results, and provides useful data to comprehend the weak points of products.

(1) Scene analysis

Scene analysis is the first activity of this validation. Scene analysis means a comparison between radiance and product. It can roughly review of the total reliability of product through this activity

(2) Climate data comparison

Comparison with climate data is an activity to identify whether the product has reliable climate data. Also, product data can figure out how it is biased. Long term data must be obtained, but this validation was limited for August, 2006. Climate data can figure out that the cause of bias for retrieval value divided and compared with a variety of conditions. For example, It compares with climate data of MODIS products for day, night, water phase clouds, ice phase clouds, southern hemisphere, northern hemisphere, Antarctic region, the tropic region, and the mid-latitude region.

(3) Time-series comparison

Time-series comparison is an activity to compare the validation of ancillary data and diurnal variation during the validation period for the region of interest. The region of interest is selected evenly on the land, ocean, desert, and various surface conditions such as snow/ice, low, middle, and high latitude. Nine regions of interest were selected in this validation; Seoul, Hwabuk plain in China, Gobi desert, Tibetan plateau, South China Sea, East Pacific, Bering Sea, and the Antarctic region. Finally, we grasp the error range in comparison with ancillary data into pixel units for cloud information.

In this validation, cloud data of MODI06 collocation 5 were used as ancillary data. The validation



Algorithm Theoretical Basis Document For Cloud Top Temperature and Pressure

Code:NMSC/SCI/ATBD/CTTP
Issue:1.0 Date:2012.12.26
File: CTP-ATBD_V5.0.hwp
Page : 1/40

region for pixel comparison was limited to the Pacific Northwest (10° - 30° N, 113° - 149° E). A lot of cyclonic eddies of this region have strong wind and a zone of spiral precipitation. A variety of cloud phases are observed to have highly developed convective activity (Kim et al. 2006). To avoid a temporal and spatial discrepancy between MODIS and JAMI images, it compared the optimal pixels within 50 km distance and 30 minutes between two images considering the path of wind. About 2,160,000 cloud pixels under this condition were used as their validation. The image pixels of JMAI are at a resolution of 4km, but cloud top height of MODIS MOD06 are at a resolution of 4km. The difference of resolution between the two image pixels can lead to uncertainty in comparison of results of these pixels.

3.4.2 Validation data

(1) CMDPS Validation (COLL/VAM)

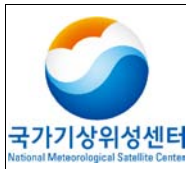
The data used to validate CMDPS cloud top height is performed using data from November 1 to November 5 of MODIS Terra and Aqua. We calculated the statistical value separated by latitude (the equator: below latitude 30° , mid-latitude: north-south 30° - 60°). This is the same with other cloud analysis data.

(2) Developer validation

JMAI radiance and the spatial resolution of the observation angle used for validation is 4km. Full-disk image is similar to location of COMS including in East Asia and western pacific, Australia, and the Antarctic region. We used MODIS cloud data to compare with products retrieved using images from JAMI. This data included cloud top height of 5km resolution for nadir (Platnick et al. 2003). This is more improved point than the previous version in collection 5 data. It is found from other references (Baum et al. 2005, King et al. 2006, Yang et al. 2007).

MODIS granules (5-min data) were collocated for the Pacific Northwest (10° - 30° N, 113° - 149° E) during the period 5-11 August 2006. MOD06 cloud top height is retrieved by the “CO₂ slicing method” (also known as the “Radiation comparison method”).

Radiation comparison method uses CO₂ absorption band between $13.2\sim 14.4\mu\text{m}$ (Menzel et al. 1983, 2006). Cloud top height has an interval of more than 10hPa between 95 hPa and 1040 hPa. This is a more delicate level than cloud top height from CMDPS retrieval. CMDPS retrieved cloud top as 50 hPa between 100hPa and 1000hPa. Daily atmospheric data (MOD08, collocation 5) of MODIS



**Algorithm Theoretical
Basis Document For
Cloud Top Temperature
and Pressure**

Code:NMSC/SCI/ATBD/CTTP
Issue:1.0 Date:2012.12.26
File: CTTP-ATBD_V5.0.hwp
Page : 1/40

gridded level-3 is collocated for the period of the same validation. MOD08 has the value of 1° pixel and is calculated by MOD06. MOD08 is the mean value cloud retrieval information during the period of validation, but it is used separately to analyze the time-series analysis for a given grid.

3.4.3 Temporal and spatial collocation method

(1) CMDPS Validation CMDPS

We collocated time and space using data of the range within -8 ~ 30 minutes on the same method as the validation of other cloud analysis algorithm. High latitude (above 60° south and north) is excluded from the validation. For temporal and spatial collocation, we excluded from the validation to represent the difference of more than 1-standard deviation in 5x5 pixels of MODIS.

(2) Developer validation

In the case of pixel comparison, CMDPS CLA criteria, it is collocated to averaged temporal and spatial pixels and entering within 30 minutes.

3.4.4 Validation result analysis

(1) CMDPS validation

Table 3 shows the result of validation from November 1 to 5, 2008. As mentioned earlier, It shows the statistical value of the correlation coefficient, bias, and RMSE of MODIS and CMDPS cloud optical thickness by a variety of validation conditions.

Table 3. Validation results of CTP

	Reference	Time	Region	R	Bias	RMSE
CTP	MODIS (MOD06)	11/1~11/5	Global	0.324	-4.256	185.795
			Low	0.261	-136.779	343.072
			Mid	0.408	19.026	144.914
	MODIS (MYD06)	11/1~11/5	Global	0.433	-7.771	176.349
			Low	0.275	-140.079	336.984
			Mid	0.554	15.93	130.135

(2) Developer validation

(1) Scene analysis

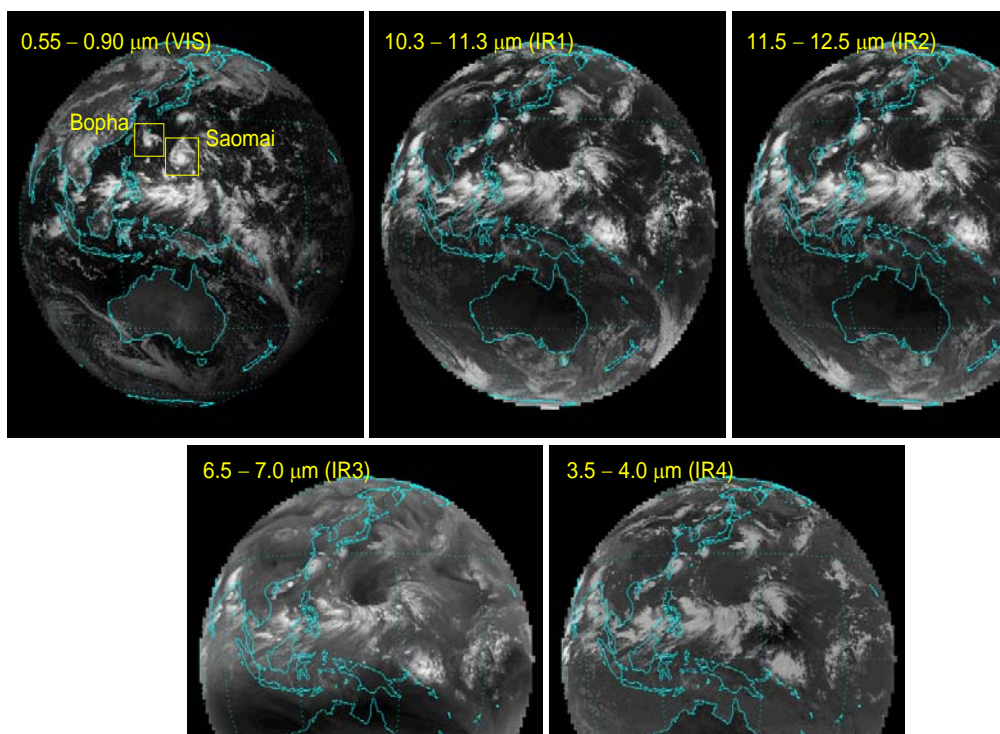



Fig. 3. JAMI/MTSAT-1R radiance imagery for the five spectral channels centered at $0.725\mu\text{m}$ (VIS), $10.8\mu\text{m}$ (IR1), $12.0\mu\text{m}$ (IR2), $6.75\mu\text{m}$ (IR3), and $3.75\mu\text{m}$ (IR4) for 0333 UTC August 7, 2006. Except for the VIS channel, the brighter color corresponds to a relatively low value in $\text{W m}^{-2} \text{sr}^{-1} \text{m}^{-1}$. The full-disk imagery covers East Asia, West Pacific, Australia, and a part of the Antarctic region ($80.5\text{S}80.5\text{N}$, $60.4\text{E}139.4\text{W}$).

Fig. 3 is an example of JAMI radiance imagery at 0333 UTC August 7, 2006. Clouds clearly show along the Intertropical convergence zone (ITCZ). Optically thick clouds by scattering of sunlight in VIS image show brightly.

Clouds for dark surface such as oceans are discriminated easily. A bright color In IR image corresponds to relatively low value, and cloud of high altitude show brightly, because they emit a lower IR radiance from the top of clouds. A high cloud with more than 400 hPa in IR3 image only shows brightly. This is because water vapor absorption happens in the troposphere of middle-low level. Low clouds in the IR window channel such as IR1 or IR2 are clearly confirmed. IR4 radiance in general has a high value for small cloud particles, and water phase particles. When it considers the

 <p>국가기상위성센터 National Meteorological Satellite Center</p>	<p>Algorithm Theoretical Basis Document For Cloud Top Temperature and Pressure</p>	<p>Code:NMSC/SCI/ATBD/CTTP Issue:1.0 Date:2012.12.26 File: CTPP-ATBD_V5.0.hwp Page : 1/40</p>
--	--	---

spectral properties of the above discussed 5 images, this time image is characterized by three great regions depending on inferred cloud properties.

(i) High clouds including clouds of Typhoon in the tropic western pacific region and optically thick clouds.

(ii) High clouds of Eastern pacific region and thin clouds.

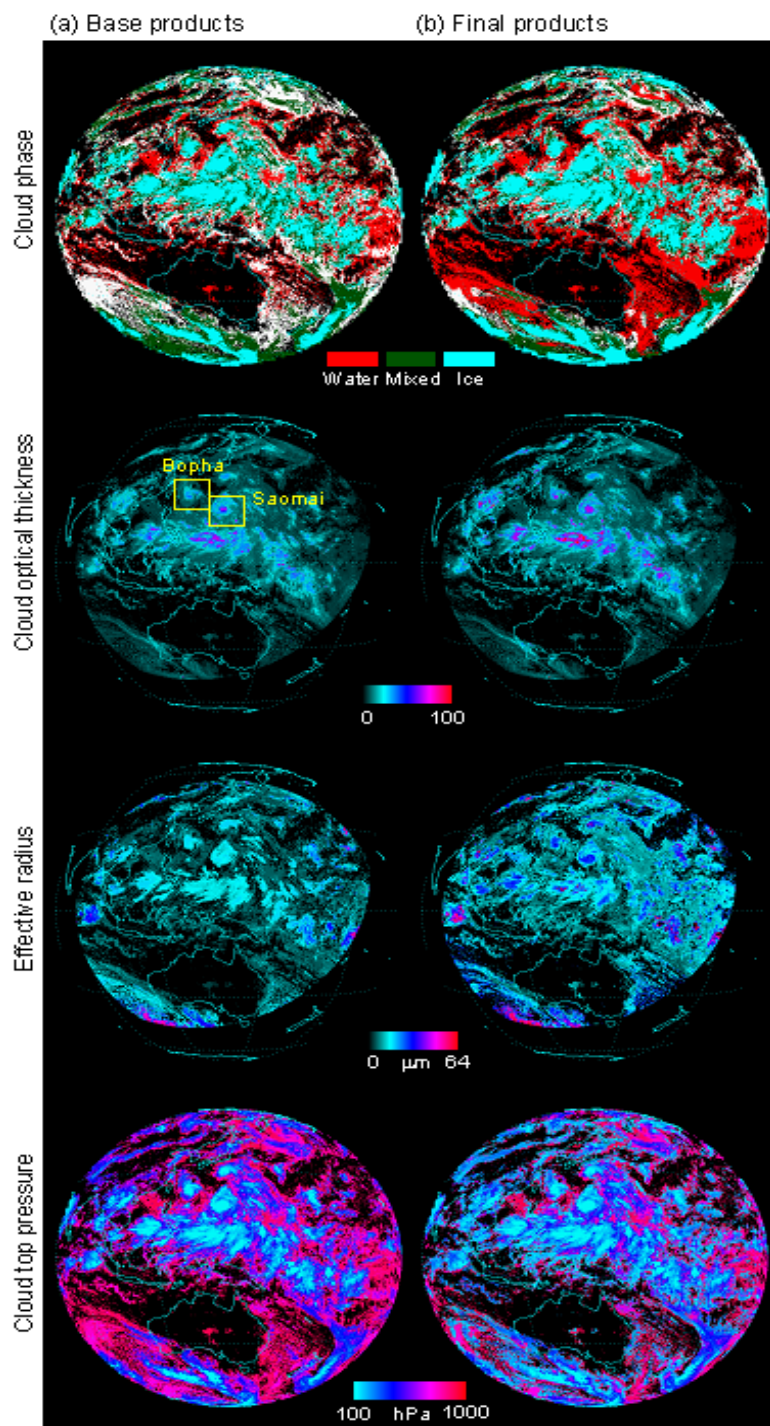
(iii) An extensive distributed region contains low and thin clouds, high and thick clouds over south-west ocean of Australia.

(i) is inferred from high VIS, low IR1, low IR2 radiance, (ii) from low VIS, low VIS, low IR2 radiance, (iii) from extensively distributed low VIS, high IR1, high IR2 radiance and high VIS, low IR3 of spatial dendrite.

We compare the inferred three properties of clouds and CMDPS algorithm products. Here we generally must review all cloud information.

Fig. 4 is a basic product (left) and final product (right) of cloud top height. Overall, the difference between the two products is clear. The final product represents the main properties of the three clouds mentioned above better than the basic product. The final cloud top height has a greater value than the basic product in ITCZ and typhoon. Very high and thick clouds of final product are more distinct in the tropic western pacific.

Fig. 4. Cloud top pressure derived by the CLA from the JAMI level-1b calibrated radiances shown in Fig. 3. Base products (left) are the results of conventional methods or without correction methods, and final products (right) from improved methods or with the correction methods developed in the present study.



(2) Comparison of Climate data

Cloud top height climate data for a month of validation period compared with MODIS (Fig. 5).



Algorithm Theoretical
Basis Document For
Cloud Top Temperature
and Pressure

Code:NMSC/SCI/ATBD/CTTP
Issue:1.0 Date:2012.12.26
File: CTTP-ATBD_V5.0.hwp
Page : 1/40

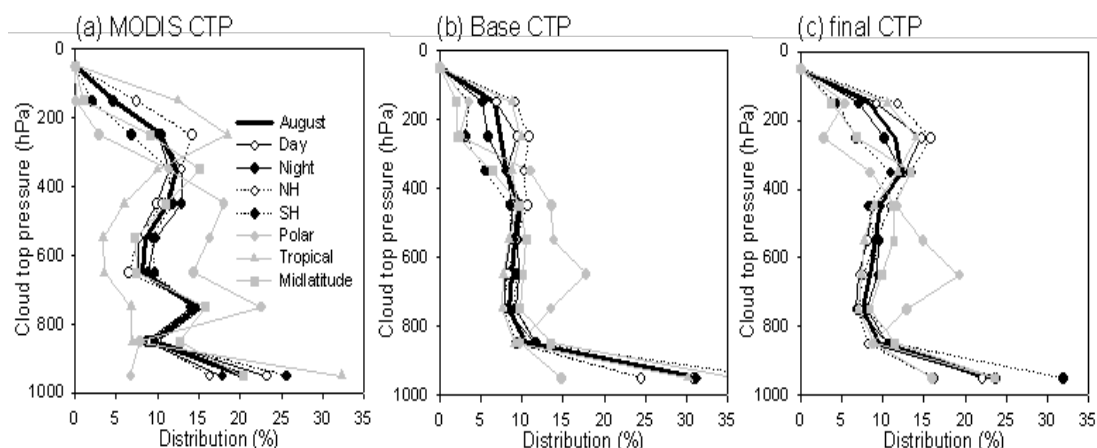
Cloud top height of MODIS has the highest frequency on August in the height of 300-400, 700-800, and 900-1000hPa. This distribution depends on day/night, Northern and Southern hemisphere, and the tropic and polar region. Basic cloud top height is similar to MODIS, but the frequency of high clouds and middle clouds are very little and cloud top height between 900 and 1000hPa has a high frequency of low clouds.

Basic cloud top height is final cloud top height to correct by radiation ratio method. In the final cloud top height, high clouds (300-400hPa) are increased by 4% and low clouds (900-1000hPa) are decreased by 7%. Consequently, the vertical distribution of final cloud top height is approximate to MODIS.

The local feature of cloud top height distribution for both Final cloud top height and MODIS cloud top height data well appear.

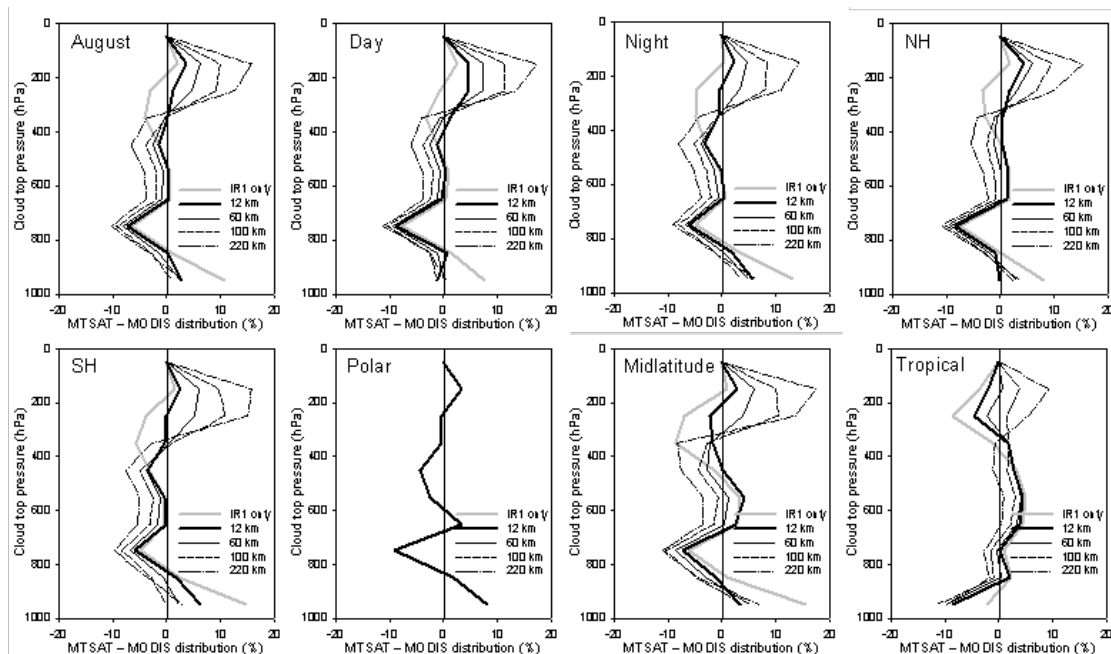
Very high (200-300hPa) clouds and very low (above 1000hPa) clouds are common in the tropic region. The middle clouds (600-800hPa) are common in the polar region. Therefore the radiation ratio method using IR1 and IR3 channels can be extremely useful to distinguish with high clouds above 400hPa. However, the radiation ratio method using MODIS CO₂ channel identified the partial middle clouds, but our algorithm can't still identify them.

Fig. 5. Relative frequency distribution (in %) of MODIS CTP (a), base CTP retrieved by the IR1 estimate only (b), and final CTP corrected by the radiance ratioing method (c) for the total clouds. The results are shown for August 2006, daytime, nighttime, Northern and Southern Hemispheres, and the polar, tropical, and midlatitude regions.



We calculated the difference of MODIS and our product to determine the uncertainty quantitatively (Fig. 6). The retrieved Basic product by IR1 displayed as a gray line. Clear sky radiance in the radiation ratio method is used and it is decided on the maximum value in clear sky pixels observed in the regular domain. It changed the domain size 12x12km, 60x60km, 100x100km, 220x220km to decide the sensitivity by domain size and retrieved the final cloud top height. These compared with the MODIS product. The larger the size of the calculated result domain, the bigger the difference with MODIS. Therefore cloud top height reduces most uncertainty for the domain of 12x12km. Therefore, the accuracy of clear sky radiance is the main factor to determine the error of cloud top height.

Fig. 6. The difference between MTSAT-1R (both base and final) CTP and MODIS CTP values (in %) shown in Fig. 5. The radiance ratios are calculated by using clear-sky radiances obtained within various spatial resolutions: 12 (3 × 3), 60 (15 × 15), 100 (25 × 25), and 220 km (55 × 55 pixels).



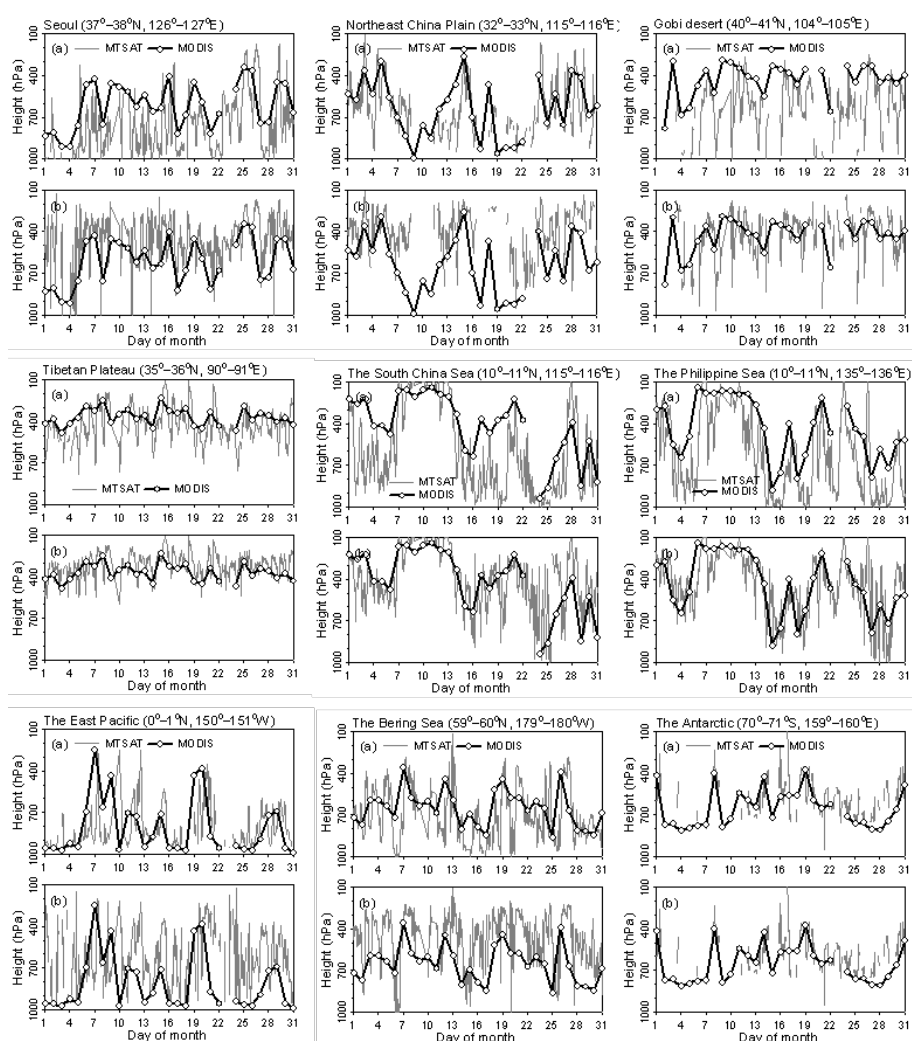
(3) Time series comparison

The climate data comparison provides very important information for validation, but it does not show the practical correspondence with MODIS product. This section analyzes the time series of products for the nine areas of interest. MTSAT product calculated every hour average for 1° pixel in comparison with MODIS gridded of MOD08 data, because it is retrieved in resolution of hourly 4km. MODIS/Terra pass at 10:30 am for all regions. Therefore, hourly MTSAT data do not exactly coincide with MODIS data and time. This is only able to identify every hour variation and a similar diurnal variation. Time series of cloud top height generally follows properties of MODIS for all analysis regions (Fig. 7). We presented as time series for basic cloud top height ((a) gray line), final cloud top height (b0 gray line), and MODIS cloud top pressure (bold line) (Fig. 7).

The underestimated cloud top height by Radiation ratio method through time series know to ascend realistically. In comparison with MODIS value, final cloud top heights are overestimated in Seoul, Northern plain of China, Eastern Pacific ocean, and the Bering Sea. The reason retrieved highly for this cloud top height, (i) middle cloud is not distinguished well, (ii) radiation ratio LUT for middle latitude is applied for latitude $30-60^\circ$, so vertical profile and real value of model for location near latitude 60° such as Bering sea are different (iii) radiation ratio in middle latitude is less sensitive to

cloud top height. The factors which cause the uncertainty exist, but final cloud height in regions such as the Gobi desert, the Tibet Plateau, the South China Sea, Philippine Sea, and the Antarctic correspond considerably with MODIS data.

Fig. 7. Time series of the ratio of ice clouds to the total clouds at nine selected sites; base CTP (a), and final CTP (b).

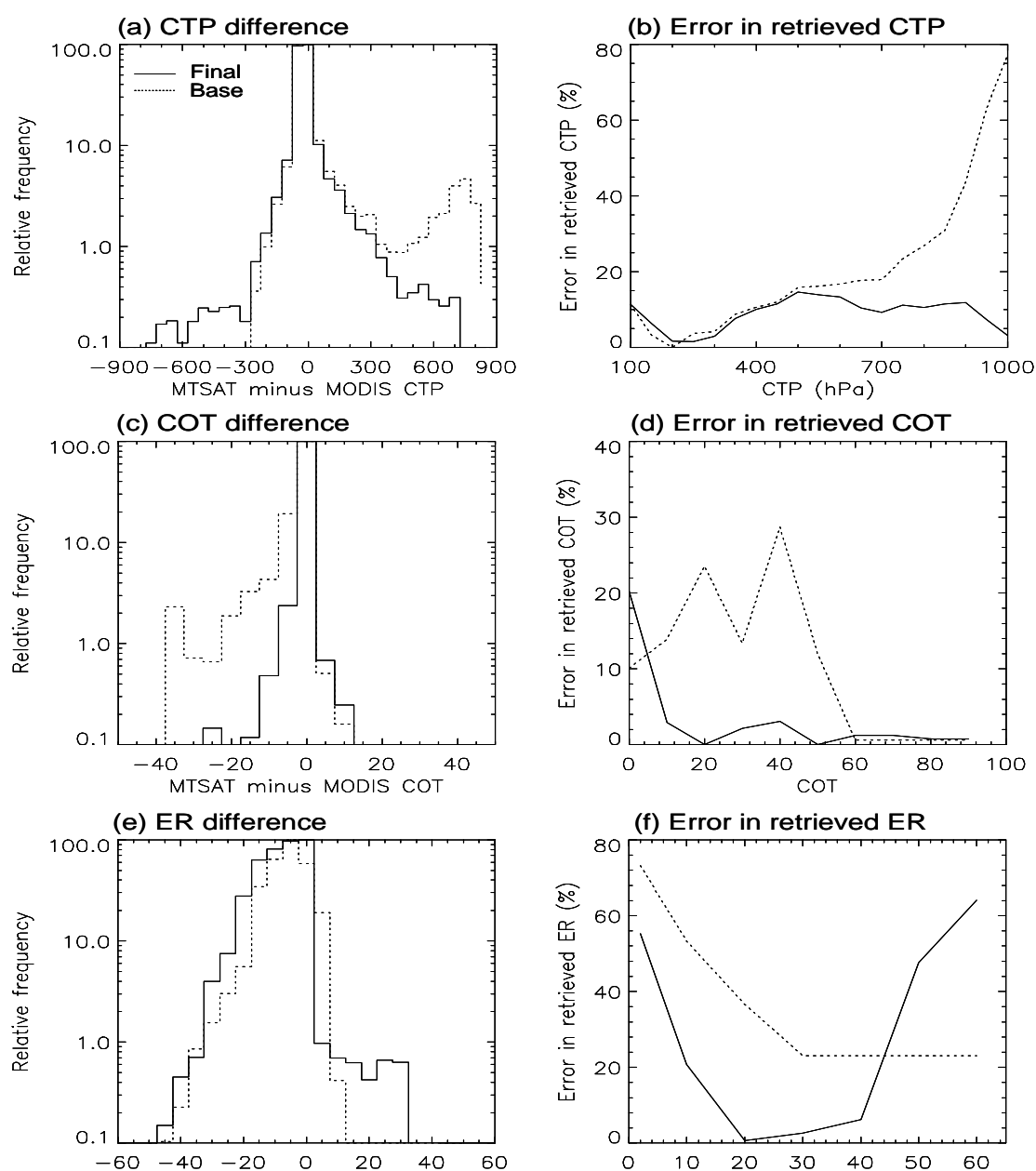


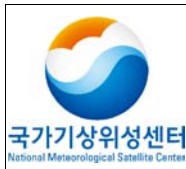
(4) Pixel comparison

Fig. 8 shows the results of pixel comparison of cloud information from MTSAT and MODIS. The figure presents Relative frequency for the maximum value of the difference between two products, and

error for MODIS data. Error was described in ratio between MTSAT minus MODIS and MODIS product.

Fig. 8. Relative frequency of MTSAT minus MODIS CTP (a) for the maximum values. Errors in the retrieved CTP (b) (in %) with respect to the corresponding parameters. The solid and dotted lines indicate values from the final (corrected) and base (uncorrected) products, respectively.





**Algorithm Theoretical
Basis Document For
Cloud Top Temperature
and Pressure**

Code:NMSC/SCI/ATBD/CTTP
Issue:1.0 Date:2012.12.26
File: CTTT-ATBD_V5.0.hwp
Page : 1/40

The whole final cloud top height and MODIS height values are consistent with each other. The difference for cloud top height below 300 hPa is present for about 0.1% of total pixels. The factor to cause the inconsistency are the difference of retrieval resolution, the radiation ratio, clear sky radiance, and atmosphere vertical profile.

In comparison with Basic cloud top height and final cloud top height, final cloud top height can know to approximate to MODIS. Especially, the error for low clouds (Cloud top height ≥ 700 hPa) decreased considerably. The error in final cloud top height is less than approximately 10%, a high cloud between 200-300hPa has the minimum value.

4 Interpretation method of the retrieval result

This algorithm retrieves cloud top height and cloud top temperature. Acc. of the retrieved data are all 1, Prec. is pressure 50, the temperature has a value of 1. The range of pressure is 100~150hPa, the temperature is 170~300K.

Table 4. Detailed Output data for the CTTT algorithm.

OUTPUT DATA						
Parameter	Mnemonic	Units	Min	Max	Prec	Acc
Cloud top temperature	cloud_top_temp	K	170	300	1	1
Cloud top pressure	cloud_top_pressure	hPa	100	1050	50	1

Prec: Precision, Acc: Accuracy, Res: Resolution

5. COMS version and algorithm improvement after COMS satellite launch

Cloud height is calculated by radiation ratio method of 6.7 μ m and 11 μ m. LUT of existing radiation ratio G value was provided as three type of middle latitude summer, the tropic, middle latitude winter based on latitude $\pm 30^\circ$.

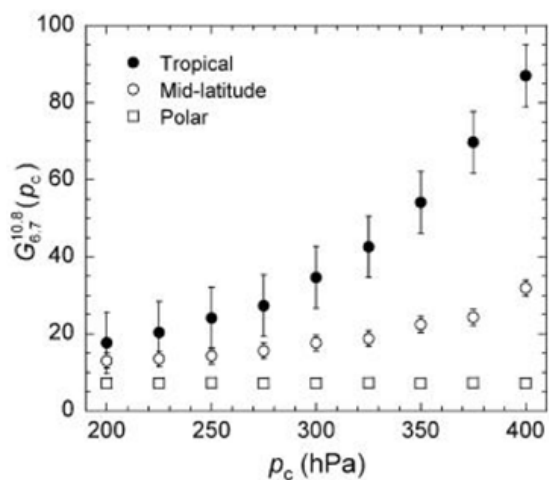


Fig. 9 Simulation for radiance ratio and single layer ice-clouds.

The discontinuities of cloud top height in latitude $\pm 30^\circ$ is found and modified it. Modified content is shown in Table 5. The result applied the new algorithm is shown in Fig. 10.

Table 5. Modification of lookup table for CMDPS CTTP

before modification	
latitude $-30^\circ \sim 30^\circ$	The tropic LUT
Winter hemisphere latitude $30^\circ \sim 90^\circ$	Middle latitude winter LUT
Summer hemisphere latitude	Middle latitude summer LUT
after modification	
Winter hemisphere latitude	Middle latitude winter LUT
Winter hemisphere latitude	Interpolation for latitude of Middle latitude winter LUT and the tropic LUT
Summer hemisphere latitude	Interpolation for latitude of Middle latitude summer LUT and the tropic LUT
Summer hemisphere latitude	Middle latitude summer LUT

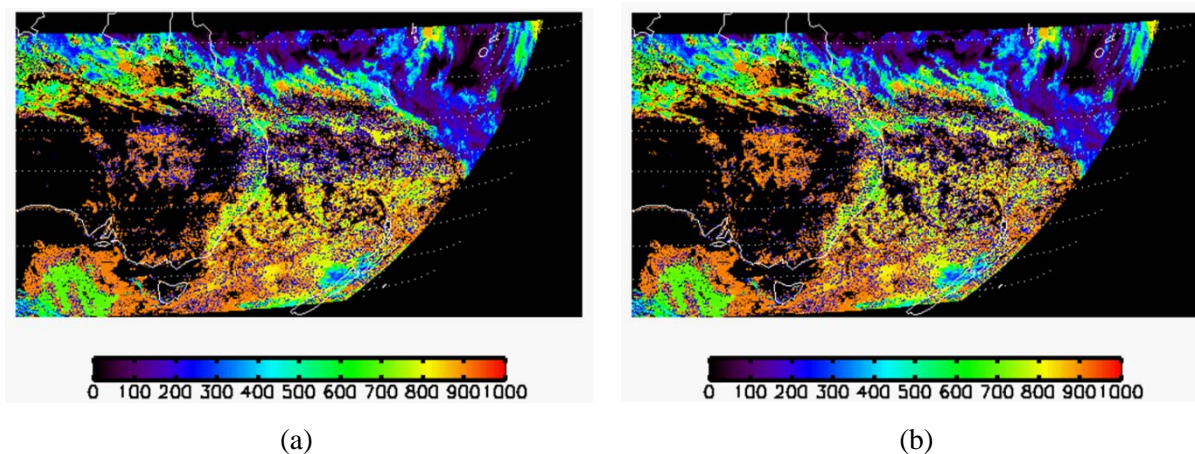


Fig. 10. Cloud top pressure (a)before and (b)after correcting discontinuities at $\pm 30^\circ$ latitude.

To improve the overestimated cloud top temperature, improved for (a) regression coefficient re-retrieval of the optimal-fit correction using single channel method, (b) LUT re-retrieval of radiation ratio method, clear sky radiance. The result of (a) is Table 6, The figure of the re-retrieved cloud top pressure is the same as Fig 11.

Table 6. Modification of regression coefficient (best-fit method)

SZA	Before modification			After modification		
	a	b	c	a	b	c
0°~10°	-0.003486	3.19251	-336.311	7.795572×10^{-6}	0.9860177	0.000000
10°~20°	-0.003474	3.18258	-334.434	7.913203×10^{-6}	0.9858522	0.000000
20°~30°	-0.003415	3.13266	-325.055	8.126994×10^{-6}	0.9855779	0.000000
30°~40°	-0.003320	3.05693	-311.247	8.572551×10^{-6}	0.9849832	0.000000

40°~50°	-0.003164	2.93879	-290.412	9.273953×10^{-5}	0.9841015	0.000000
50°~60°	-0.002934	2.77426	-262.283	0.0001038601	0.9827880	0.000000
60°~70°	-0.002679	2.59754	-232.622	0.0001201152	0.9809093	0.000000
70°~80°	-0.002360	2.36972	-193.661	0.0001484903	0.9775916	0.000000
80°~90°	-0.001991	2.11005	-149.727	0.0002151845	0.9681243	0.000000

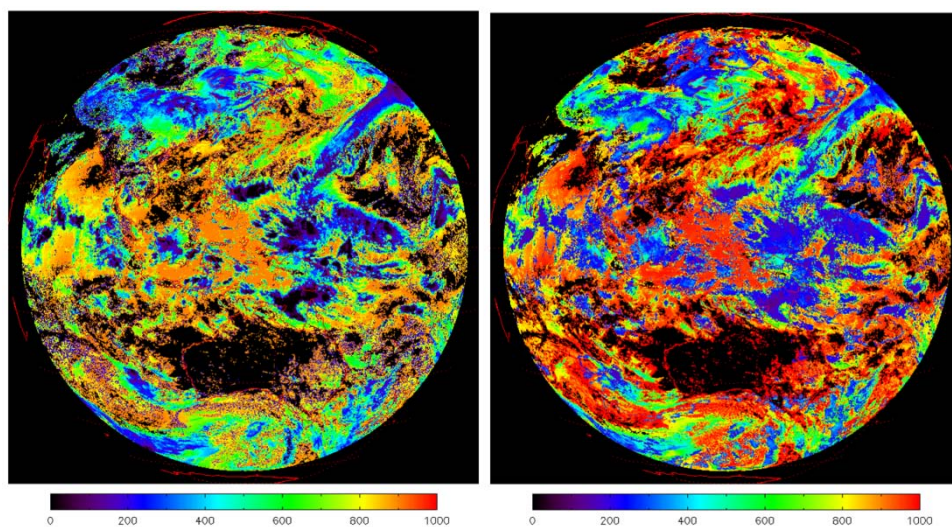


Fig. 11 Cloud top pressure (a)before and (b)after modifying coefficient, lookup table, and definition of clear sky radiance

6. Problems and possibilities for improvement

We need to diversify validation information for user-centered algorithm improvement. For example, we must provide the user with a variety of information analyzing day/night, Southern / Northern hemispheres, latitude, Height separation (high uncertainty of high latitude and middle clouds) errors and relationship with CTTP.

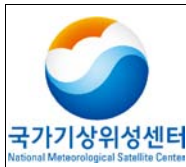


Algorithm Theoretical
Basis Document For
Cloud Top Temperature
and Pressure

Code:NMSC/SCI/ATBD/CTTP
Issue:1.0 Date:2012.12.26
File: CTP-ATBD_V5.0.hwp
Page : 1/40

7. References

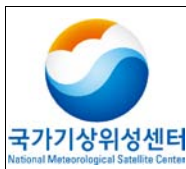
- Baum, B.A., Yang, P., Heymsfield, A.J., Platnick, S., King, M.D., Hu, Y.X. and Bedka, S.T., 2005, Bulk scattering properties for the remote sensing of ice clouds. Part II: Narrowband models. *Journal of Applied Meteorology*, 44, pp. 1896–1911.
- Choi, Y.-S., Ho, C.-H. and Sui, C.-H., 2005, Different optical properties of high cloud in GMS and MODIS observations. *Geophysical Research Letters*, 32, L23823, doi:10.1029/2005GL024616.
- Choi, Y.-S. and Ho., C.-H., 2006, Radiative effect of cirrus with different optical properties over the tropics in MODIS and CERES observations. *Geophysical Research Letters*, 33, L21811, doi:10.1029/2006GL027403.
- Choi, Y.-S., Ho, C.-H., Ahn, M.-H. and Kim, Y.-M., 2007, An exploratory study of cloud remote sensing capabilities of the Communication, Ocean and Meteorological Satellite (COMS) Imagery. *International Journal of Remote Sensing*, 28, pp. 4715-4732.
- Kim, J.-H., Ho, C.-H., Lee, M.-H., Jeong, J.-H. and Chen, D., 2006, Large increase in heavy rainfall associated with tropical cyclone landfalls in Korea after the late 1970s. *Geophysical Research Letters*, 33, L18706, doi:10.1029/2006GL027430.
- King, M.D., Platnick, Hubanks, P.A., Arnold, G.T., Moody, E.G., Wind, G., and Wind, B., 2006, Collection 005 Change Summary for the MODIS Cloud Optical Property (06_OD) Algorithm. Available online at: modis-atmos.gsfc.nasa.gov/C005_Changes/C005_CloudOpticalProperties_ver311.pdf.
- Liou, K.N., 2002, *An introduction to atmospheric radiation* 2nd ed.. Academic Press, San Diego.
- Menzel, W.P., Smith, W.L. and Stewart, T.R., 1983, Improved cloud motion wind vector and altitude assignment using VAS. *Journal of Climate and Applied Meteorology*, 22, pp. 377–384.
- Menzel, W.P., Frey, R.A., Baum, B.A. and Zhang, H., 2006, Cloud top properties and cloud phase algorithm theoretical basis document, In *MODIS Algorithm Theoretical Basis Document*, NASA.
- Platnick, S., King, M.D., Ackermann, S.A., Menzel, W.P., Baum, B.A., Riedi, J.C. and Frey, R.A., 2003, The MODIS cloud products: Algorithms and examples from Terra. *IEEE Transactions on Geoscience and Remote Sensing*, 41, pp. 456-473.
- Rossow, W.B. and Garder, L.C., 1993a, Cloud detection using satellite measurements of infrared and



Algorithm Theoretical
Basis Document For
Cloud Top Temperature
and Pressure

Code:NMSC/SCI/ATBD/CTTP
Issue:1.0 Date:2012.12.26
File: CTPP-ATBD_V5.0.hwp
Page : 1/40

- visible radiances for ISCCP. *Journal of Climate*, 6, pp. 2341–2369.
- ____ and _____, 1993b, Validation of ISCCP cloud detections. *Journal of Climate*, 6, pp. 2370–2393.
- ____, Walker, A.W. and Garder, L.C., 1993, Comparison of ISCCP and other cloud amounts. *Journal of Climate*, 6, pp. 2394–2418.
- ____ and Schiffer, R.A., 1999, Advances in understanding clouds from ISCCP. *Bulletin of the American Meteorological Society*, 80, pp. 2261–2287.
- Shupe, M.D., Matrosov, S.Y. and Uttal, T., 2006, Arctic mixed-phase cloud properties derived from surface-based sensors at SHEBA. *Journal of the Atmospheric Sciences*, 63, pp. 6977–7111.
- Strabala, K.I., Ackerman, S.A. and Menzel, W.P., 1994, Cloud properties inferred from 8–12- μ m data. *Journal of Applied Meteorology*, 33, pp. 212–229.
- Yang, P., Zhang, L., Hong, G., Nasiri, S.L., Baum, B.A., Huang, H.L., King, M.D. and Platnick, S., 2007, Differences between collection 4 and 5 MODIS ice cloud optical/microphysical products and their impact on radiative forcing simulations. *IEEE Transactions on Geoscience and Remote Sensing*, 45, pp. 2886–2899.
- Verlinda, J. and Coauthors, 2007, The mixed-phase arctic cloud experiment. *Bulletin of the American Meteorological Society*, 88, pp. 2052–2111.



Algorithm Theoretical Basis Document For Cloud Top Temperature and Pressure

Code:NMSC/SCI/ATBD/CTTP
Issue:1.0 Date:2012.12.26
File: CTTT-ATBD_V5.0.hwp
Page : 1/40

8. Appendix

International Journal of Remote Sensing
Vol. 28, No. 21, 10 November 2007, 4715–4732



An exploratory study of cloud remote sensing capabilities of the Communication, Ocean and Meteorological Satellite (COMS) imagery

Y.-S. CHOI†, C.-H. HO*‡, M.-H. AHN‡ and Y.-M. KIM†

†Climate Physics Laboratory, School of Earth and Environmental Sciences, Seoul
National University, Seoul 151–742 Korea

‡Meteorological Research Institute, Korea Meteorological Administration, Seoul,
Korea

(Received 8 February 2006; in final form 24 January 2007)

The present study documents optimal methods for the retrieval of cloud properties using five channels (0.6, 3.7, 6.7, 10.8 and 12.0 μm) that are used in many geostationary meteorological satellite observations. Those channels are also to be adopted for the Communication, Ocean and Meteorological Satellite (COMS) scheduled to be launched in 2008. The cloud properties focused on are cloud thermodynamic phase, cloud optical thickness, effective particle radius and cloud-top properties with specific uncertainties. Discrete ordinate radiative transfer models are simulated to build up the retrieval algorithm. The cloud observations derived from the Moderate-resolution Imaging Spectroradiometer (MODIS) are compared with the results to assess the validity of the algorithm. The preliminary validation indicates that the additional use of a band at 6.7 μm would be better in discriminating the cloud ice phase. Cloud optical thickness and effective particle radius can also be produced up to, respectively, 64 and 32 μm by functionally eliminating both ground-reflected and cloud- and ground-thermal radiation components at 0.6 and 3.7 μm . Cloud-top temperature (pressure) in ± 3 K (± 50 hPa) uncertainties can be estimated by a simple 10.8- μm method for opaque clouds, and by an infrared ratioing method using 6.7 and 10.8 μm for semitransparent clouds.

1. Introduction

Clouds are of continual interest because they provide a visible indication of what is going on in the atmosphere. Clouds play an important role in the Earth's climate and could be a crucial factor in evaluating the strength of global warming (see, for example, Lindzen *et al.* 2001, Hartman and Michelsen 2002, Choi *et al.* 2005a, Choi and Ho 2006). Knowledge of such a role requires development of the observational techniques applied to precise satellite measurements. Remote sensing of cloud properties has been studied focusing largely on the applications of the spectral bands of onboard radiometers. In the past few years, cloud analysis techniques have been considerably improved with the advent of Moderate-resolution Imaging Spectroradiometer (MODIS) instruments. The MODIS provides information on a variety of cloud properties by using spectral radiances at 36 visible and infrared (IR) bands (King *et al.* 1997, Baum *et al.* 2000). The detection of cirrus clouds has been particularly enhanced in MODIS by incorporating a band at 1.38 μm , which lies in

*Corresponding author. Email: hoch@cpl.snu.ac.kr



Algorithm Theoretical Basis Document For Cloud Top Temperature and Pressure

Code: NMSC/SCI/ATBD/CTTP
Issue: 1.0 Date: 2012.12.26
File: CTTP-ATBD_V5.0.hwp
Page : 1/40

COMS cloud analysis algorithm

4721

stage of phase decision (table 2). In detail, cloud pixels pass the stage of the ice phase decision first. At this stage, the three tests judge whether the pixel is composed of ice particles or not. If the pixel is not identified as ice, it passes on to the next tests using $BT_{10.8}$ and $BT_{6.7}$ for the mixed phase. If the pixel does not satisfy the criteria of being in the mixed phase, it will go through to the next stage using $BT_{10.8}$ and $BT_{6.7}$ for the water phase. Finally, the pixel unclassified as any phase category will be assigned to an unknown phase.

An effect of missing an 8.7- μm band in the IR trispectral method of the MODIS can be found by comparison of the MODIS cloud phase with that which has been newly retrieved by a $BT_{8.7}$ -free algorithm (i.e. only using 10.8 and 12.0 μm). Table 3 shows that a large portion of the ice clouds are not well distinguished by the $BT_{8.7}$ -free algorithm; the MODIS ice phase takes 40.8% of the total clouds whereas that from the $BT_{8.7}$ -free algorithm takes only 15.6%. Moreover, the MODIS ice phase is in less agreement with that from the $BT_{8.7}$ -free algorithm (15.6% in table 3). More than half of the scenes identified as ice clouds in MODIS are distinguished as mixed phases in the $BT_{8.7}$ -free algorithm (21.2% vs. 40.8% in table 3).

The effect of adding a 6.7- μm band to the $BT_{8.7}$ -free algorithm was also examined in a similar manner, and the results are presented in parentheses in table 3. It can be seen that the MODIS ice phase pixels are easily detected in the $BT_{6.7}$ algorithm (i.e. using 6.7, 10.8 and 12.0 μm). Specifically, MODIS data on detection of ice pixels are in 29.6% agreement with those from the $BT_{6.7}$ algorithm, which takes 72.5% of the total MODIS ice phase. The total percentage of ice phase increased up to 32.5%. This is a considerable improvement compared to the results from the previous $BT_{6.7}$ -free algorithm. Those results account for the fact that large cloud regions comprising ice particles can be identified more accurately by their low $BT_{6.7}$ values, although cloud phases over the regions are not distinguishable through the $BT_{10.8}$ and $BTD_{10.8-12.0}$ threshold tests. Thus, detection of the ice phase using only $BT_{10.8}$ and $BT_{12.0}$ can cause serious problems in that a large portion of such ice clouds can be overlooked. To summarize, we have demonstrated that the 6.7- μm band can be a useful alternative in the case of a missing 8.7- μm band.

4. Cloud optical thickness (τ_c) and effective particle radius (r_e)

Since the determination of the scaled τ_c using a nonabsorbing visible wavelength 0.6- μm band was introduced by King (1987), the method has been used operationally for GMS-5 (Okada *et al.* 2001). τ_c is solely retrieved by this method because the near-IR channel is not available. Here, GMS-5 assumed the effective particle radius

Table 3. Comparison of cloud phase from the MODIS IR trispectral algorithm and from the algorithm for the COMS, as described in table 2. The numbers (in parentheses) designate those from the algorithm from which $BT_{6.7}$ is excluded (included).

COMS	MODIS					Total
	Clear	Water	Mixed	Ice	Uncertain	
Clear	13.0	0.0	0.0	0.0	0.0	13.0
Water	0.0	11.5 (19.7)	0.0	0.1 (0.3)	0.9 (4.1)	12.5 (24.1)
Mixed	0.0	2.3 (2.2)	7.1 (5.5)	21.2 (8.4)	5.8 (5.1)	36.4 (21.2)
Ice	0.0	0.0 (0.3)	0.0 (1.6)	15.6 (29.6)	0.0 (1.0)	15.6 (32.5)
Uncertain	0.0	13.8 (3.9)	0.0	3.9 (2.5)	4.9 (2.9)	22.6 (9.3)
Total	13.0	27.7	7.1	40.8	11.5	100.0

represents minimum (maximum) values for water (ice) clouds. The cloud water (ice)

of all clouds to be $10\ \mu\text{m}$. Later, the retrieval method for both τ_c and r_e (also called the sun reflection method) was developed by combining water-absorbing near-IR wavelengths such as 1.6 , 2.2 and $3.7\ \mu\text{m}$ with the reflected radiance at $0.6\ \mu\text{m}$ (Nakajima and King 1990, Nakajima and Nakajima 1995 (hereafter NN), and many other studies). Unlike 1.6 and $2.2\ \mu\text{m}$, however, the radiance at $3.7\ \mu\text{m}$ contains large thermal components emitted from both the surface and the cloud top. The removal of the thermal components leads to importing other variables such as T_g and T_c , so that the accuracy of the products may decrease depending on these factors. For that reason, the algorithm of MODIS uses the near-IR $2.2\ \mu\text{m}$ band, which is free of such components, together with visible 0.6 or $0.8\ \mu\text{m}$ (King *et al.* 1997).

Although a $3.7\text{-}\mu\text{m}$ band has undesirable components for the sun reflection method, retrieval of τ_c and r_e by making use of 0.6 and $3.7\ \mu\text{m}$ seems to be practical. Figures 2(a) and 2(b) show the dependence of MODIS-retrieved τ_c and r_e , respectively, on both 0.6- and $3.7\text{-}\mu\text{m}$ radiances. The 30 000 observed radiances over the ocean obtained in this study were plotted after being classified by the coincident values of τ_c and r_e . In figure 2, the various symbols correspond to the radiance averages for each τ_c and r_e category, and the error bars show the ranges of the radiance that each of τ_c and r_e categories can have. The pixels used in figure 2 are constrained to have the same angular variables (θ , θ_0 , ϕ) to avoid angular dependence on the radiance from the cloud layer with τ_c (or r_e). As mentioned above, MODIS-retrieved τ_c and r_e are values derived from mainly $0.6\ \mu\text{m}$ ($0.8\ \mu\text{m}$) and $2.2\ \mu\text{m}$ over land (sea). Nevertheless, figure 2 clearly shows that the cloud with a larger τ_c (r_e) has a greater (smaller) $0.6\text{-}\mu\text{m}$ ($3.7\text{-}\mu\text{m}$) radiance.

Figure 3 shows the RT model SBDART simulation of clouds with a variety of τ_c and r_e for 0.6- , 1.6- , 2.2- and $3.7\text{-}\mu\text{m}$ radiances under the condition of specific angular variables. Similar figures are shown in many studies (e.g. NN, King *et al.* 1997). The sensitivity of the nonabsorbing and absorbing channels to τ_c and r_e is almost orthogonal for optically thick clouds ($\tau_c \geq 16$). For optically thin clouds ($\tau_c < 16$), the sensitivity of the $0.6\text{-}\mu\text{m}$ and $2.2\text{-}\mu\text{m}$ (or $3.7\text{-}\mu\text{m}$) channels is more orthogonal than that of the $1.6\text{-}\mu\text{m}$ channel (figure 3). This orthogonality ensures independent retrieval of τ_c and r_e (King *et al.* 1992). However, the intensity (i.e. radiance) at $3.7\text{-}\mu\text{m}$ itself is 10 digits smaller in comparison to other absorbing channels. Thus, using $3.7\ \mu\text{m}$ requires a highly sensitive manipulation to prevent a large uncertainty in the retrieved τ_c and r_e .

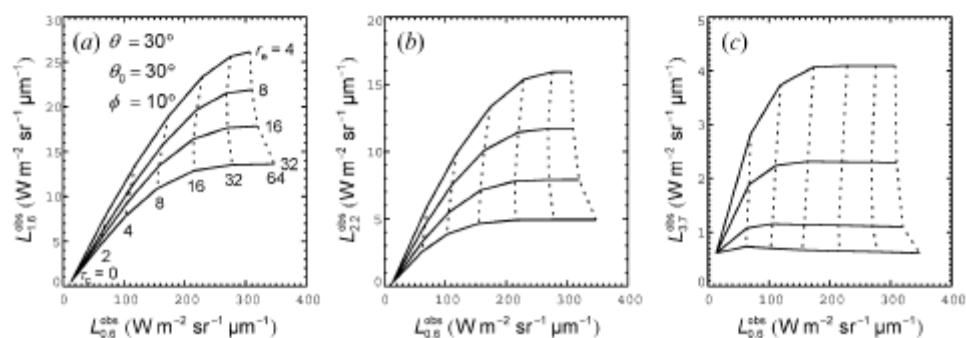


Figure 3. Comparison of (a) 1.6- , (b) 2.2- and (c) $3.7\text{-}\mu\text{m}$ radiances as a function of τ_c (0, 2, 4, 8, 16, 32, 64) and r_e (4, 8, 16, 32) with the angular variables of $\theta=30^\circ$, $\theta_0=30^\circ$ and $\phi=10^\circ$.



Algorithm Theoretical Basis Document For Cloud Top Temperature and Pressure

Code:NMSC/SCI/ATBD/CTTP
Issue:1.0 Date:2012.12.26
File: CTP-ATBD_V5.0.hwp
Page : 1/40

COMS cloud analysis algorithm

4723

The sun reflection method using 0.6 and 3.7 μm has been discussed previously by NN for the AVHRR. The method uses solar radiation only, reflected by cloud layer, and accompanies an essential process to undertake decoupling undesirable radiation components: (1) ground-reflected radiation, (2) cloud and ground thermal radiation. Based on the RT theory for plane-parallel layers with an underlying Lambertian surface (refer to NN), the decoupled radiances for 0.6- and 3.7- μm wavelengths are given simply as follows:

$$L_{0.6} = L_{0.6}^{\text{obs}} - L_{0.6}^{\text{sr}} \quad (1)$$

$$L_{3.7} = L_{3.7}^{\text{obs}} - L_{3.7}^{\text{sr}} - L_{3.7}^{\text{th}} \quad (2)$$

where L^{obs} is the satellite-received radiance, L^{sr} the ground-reflected radiance, and L^{th} the cloud and ground thermal radiance. The radiance is a function of τ_c , r_e , θ , θ_0 and ϕ . The cloud fraction reduces L^{obs} if a pixel is partially cloudy, which will consequently cause an underestimation of τ_c . Because there is not yet any method for completely picking out such partial-cloudy pixels, we assume that cloudy pixels are fully overcast in equations(1) and (2). NN designed an iterative algorithm that starts from initial values such as $\tau_c=35$, $r_e=10 \mu\text{m}$ and $Z=2 \text{ km}$, where Z is the cloud-top height. They used preprocessed data; cloud-reflected radiance and reflectivity (at 0.6 and 3.7 μm), and transmissivity (at 0.6, 3.7 and 10.8 μm) (see NN for details). In brief, their algorithm compared model radiance with calculated radiance (observed radiance minus undesirable components), and it was iterated until exact values of τ_c and r_e were found.

This method is certainly applicable to the COMS algorithm because it has all the channels needed. However, the NN method requires too many assumptions to compute the undesirable components, as follows. First, cloud geometric thickness (D) is obtained from the relation $D=W/w$, where W and w are, respectively, the liquid water content and the liquid water path. In this calculation, W is led by the assumed formation (equation(11) of NN), and climatological w is simply used for five classified cloud types. At this point, cloud types must be an input, which complicates the algorithm. Second, Z is obtained by an assumed relationship with a constant lapse rate of 6.5 K km^{-1} . Third, 10.8- μm transmissivity (t) is derived with Z and the estimated D by a pre-calculated lookup table. Here, the use of a lookup table, as well as two other lookup tables, can increase numerical uncertainty. Fourth, T_g must be determined together with A_g , then T_c is determined with the previously derived T_g , A_g and t . Here, T_g for a cloud-free pixel adjacent to the target cloudy pixels may be another source of uncertainty in the calculation of T_c when clouds cover a large area.

To overcome those limitations, we did not carry out the calculation of D with initial Z or that of t , T_g and T_c , which were necessary parameters to get the undesirable radiation components in NN's method. Instead, observed radiances were explicitly decoupled from undesirable radiation components that were estimated by the direct use of climatological A_g and 10.8- μm radiance by equations(3) and (4), respectively. Ground-reflected radiance L_i^{sr} at i channel (e.g. 3.7 or 10.8 μm) can be estimated by

$$\begin{aligned} L_i^{\text{sr}} &\cong A_g L_i^{\text{sr}} (A_g = 1) \\ &= A_g [(L_i + L_i^{\text{sr}} (A_g = 1)) - (L_i + L_i^{\text{sr}} (A_g = 0))] \end{aligned} \quad (3)$$

where the multiple reflection between the ground surface and the upper layer is assumed to be very small, then L_i^{sf} changes almost linearly in proportion to A_g according to the RT theory applied to equations(1) and (2). We can further derive an extended formula, as shown in figure 3, with respect to thermal-free radiance, which is the sum of cloud- and ground-reflected radiances ($L_i + L_i^{sf}$). Note that L_i^{sf} is zero for $A_g=0$ and that L_i is cancelled out in the extended formula of equation (3). The RT simulation results in figures 2 and 3 of NN supporting the linear increase of thermal-free radiance at both 0.6- and 3.7- μm bands. On the basis of the extended form of equation(3), we can use only one lookup table, which contains the angular variables and their corresponding thermal-free radiances for two reference values of A_g (0 and 1) and for a variety of τ_c (0 to 64) and r_e (0 to 32 μm). Once angular variables and A_g are known, the simulated thermal-free radiance for $A_g=0$ is subtracted from that for $A_g=1$ in the lookup table and multiplied by a given A_g (equation(3)).

Cloud and ground thermal radiance at 3.7 μm is obtained from the following:

$$L_{3.7}^{\text{th}} \cong a \cdot L_{10.8}^{\text{obs}2} + b \cdot L_{10.8}^{\text{obs}} + c \quad (4)$$

where $L_{10.8}^{\text{obs}}$ is the 10.8- μm satellite-received radiance, and a , b and c are regression coefficients. Equation(4) is based on the hypothesis that both $L_{3.7}^{\text{th}}$ and $L_{10.8}^{\text{obs}}$ are proportional to the Planck function of T_g and T_c . In this relationship, the different transmissivities of the atmosphere and the cloud layer, and a ground emissivity between 3.7 and 10.8 μm , would give rise to regression errors as shown in figure 4. The figure shows the result of the SBDART calculation for the sensitivity of the thermal radiance $L_{3.7}^{\text{th}}$ to $L_{10.8}^{\text{obs}}$. The calculations are carried out for clouds with a variety of τ_c (0–64) and r_e (0–32 μm) under diverse T_c (220–290 K) and T_g (250–300 K). The value of $L_{3.7}^{\text{th}}$ increases with the second-order polynomial relation when $L_{10.8}^{\text{obs}}$ increases. The mean error range of $L_{3.7}^{\text{th}}$ for all the $L_{10.8}^{\text{obs}}$ values is about $0.02 \text{ W m}^{-2} \mu\text{m}^{-1} \text{ sr}^{-1}$, which causes 2% uncertainty in the final r_e . In addition, this

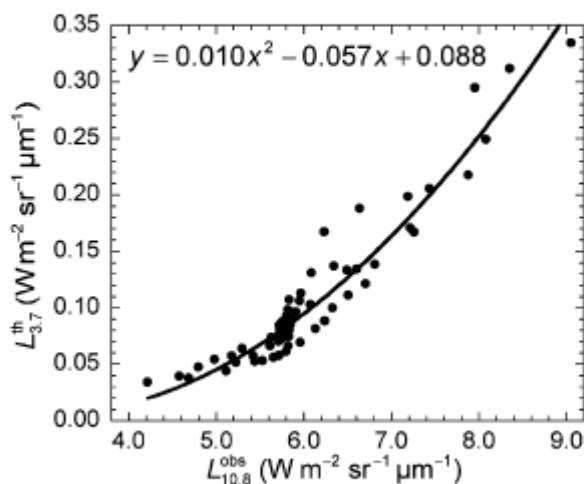


Figure 4. Sensitivity of 3.7- μm thermal radiances ($L_{3.7}^{\text{th}}$) to 10.8- μm satellite-received radiances ($L_{10.8}^{\text{obs}}$) for the clouds with a variety of τ_c (0 to 64) and r_e (0 to 32 μm) under diverse T_c and T_g . The solid line is the second-order polynomial regression line of the plots.

decoupling method indicates, in figure 4, that the error of $L_{3.7}^{\text{th}}$ would be even larger for cold surfaces (i.e. cold $L_{10.8}^{\text{obs}}$). Taking into account the fact that NN's method needed many lookup tables to obtain the thermal radiance as a function of many factors such as cloud albedo, t , A_g , T_g and T_c , the decoupling method using such a simple relationship between $L_{3.7}^{\text{th}}$ and $L_{10.8}^{\text{obs}}$ is fairly effective in time. Finally, we removed undesirable components from the observed radiance by equations (1) and (2) with the aid of equations (3) and (4).

Figures 5(a) and 5(b) respectively show a comparison of τ_c and r_e from the new algorithm with those of MODIS. τ_c from the new algorithm is in fairly good agreement with MODIS τ_c for optically thin clouds ($\tau_c < 20$). For thick clouds, τ_c deviates even more from the linear relationship (figure 5(a)). The mean root-mean-square errors of τ_c for thin and thick clouds are 1.39 and 5.38, respectively. This low accuracy for thick clouds results from $L_{0.6}$ itself increasing slightly for a constant r_e when the τ_c increases above 20, as shown in the RT result of figure 3. However, r_e from the new algorithm is in accord with MODIS r_e for small particles ($r_e < 12 \mu\text{m}$). For large particles, the deviation in r_e is increased for similar reasons to those stated above for τ_c . Namely, $L_{3.7}$ itself decreases slowly when r_e increases above about $12 \mu\text{m}$ (see figure 3). The mean root-mean-square errors in r_e for small and large particles are 0.83 and $1.76 \mu\text{m}$, respectively (figure 5(b)).

5. Cloud-top temperature (T_c) and pressure (p_c)

The IR-window channel estimate is the typical method in which $BT_{10.8}$ is compared with a vertical temperature profile in the area of interest. It is assumed that the cloud is opaque and fills the field of view (FOV). This is inaccurate for semi-transparent cirrus and small-element cumulus clouds (Menzel *et al.* 1983). To obtain the criterion of τ_c proper for the IR-window channel estimate, we simply depict $BT_{10.8}$ and T_c in MODIS (figure 6). Here, it is clear that T_c of an optically thick cloud ($\tau_c > 10$) has a nearly linear relationship with its $BT_{10.8}$. For the same angular conditions, an optically thick cloud with a lower T_c theoretically emerges with a

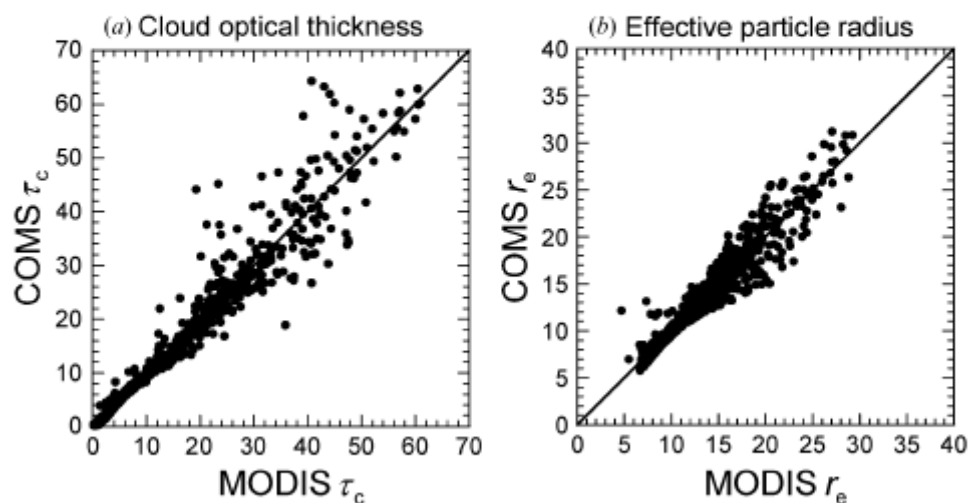


Figure 5. Comparison between MODIS-retrieved and COMS-retrieved (a) cloud optical thickness (τ_c) and (b) effective particle radius (r_e).

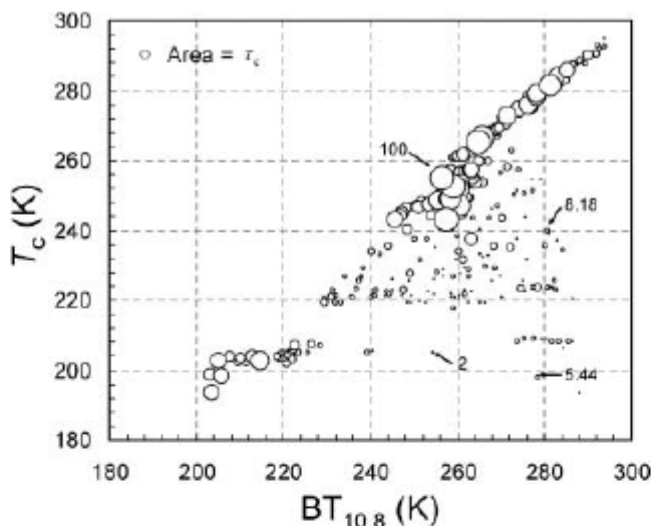


Figure 6. Scatter plots depicted from MODIS-retrieved T_c and its corresponding $BT_{10.8}$ for clouds ($\tau_c > 2$). The circles are sized by cloud optical thickness.

lower radiance at $10.8 \mu\text{m}$. The $BT_{10.8}$ from the high semitransparent clouds is generally contaminated by underlying clouds or surfaces. This is shown by the fact that $BT_{10.8}$ is greater than T_c in figure 6. To alleviate this discrepancy, a radiance rationing method has been developed and used for operational purposes (see, for example, Smith and Platt 1978, Menzel *et al.* 1983).

The idea of using the ratio of the cloud signal for two CO_2 channels viewing the same FOV to determine the p_c appeared in Smith and Platt (1978). Menzel *et al.* (1983) further described this method in detail. Wylie *et al.* (1994) used this method to determine cirrus cloud statistics from NOAA's polar-orbiting High-Resolution Infrared Radiation Sounder multispectral data in terms of cloud cover, height and effective emissivity. The window channel has also been involved in the radiance rationing method together with the sounding channels (6.2 , 7.3 and $13.4 \mu\text{m}$) to retrieve the p_c of thin clouds for SEVIRI (Le Gléau 2005).

The COMS Imager has limited channels for importing the radiance rationing method, so that only the IR-window channel ($10.8 \mu\text{m}$) and one sounding channel ($6.7 \mu\text{m}$) are available. Thus, it is necessary to evaluate this method with the two available channels. All the equations for this method are the same as those derived in Menzel *et al.* (1983). We show the relationship between the ratio ($G_{6.7}^{10.8}$) and p_c as follows.

$$G_{6.7}^{10.8}(p_c) \cong \frac{L_{10.8}^{\text{cd}} - L_{10.8}^{\text{clr}}}{L_{6.7}^{\text{cd}} - L_{6.7}^{\text{clr}}} \quad (5)$$

where L^{clr} and L^{cd} are the radiances of clear-sky and cloudy-sky, respectively. We assumed here that cloud emissivities at the two channels are near unity. It should be noted that $6.7\text{-}\mu\text{m}$ is a strong water vapour absorbing channel, so that its maximum value of weighting function is located at an altitude of around 400 hPa. Thus, $G_{6.7}^{10.8}$ in equation (5) can be applied only to high clouds with $p_c \leq 400$ hPa. Multilayer cloud systems in which an upper semitransparent cloud layer exists over an underlying opaque cloud ($p_c > 500$ hPa) layer will not lead to an overestimation of

the p_c of the semitransparent cloud, contrary to the CO₂ slicing method of MODIS (King *et al.* 1992).

Figure 7 shows the RT model Streamer simulation of $G_{6.7}^{10.8}$ for single-layer ice clouds located at 200–400 hPa. This is calculated under the conditions of $\theta=30^\circ$ for the tropical, mid-latitude and polar atmospheric profiles. The ice clouds are assumed to be composed of spherical particles. Each ratio is computed by the regression of 16 cases for various τ_c (0.5, 1, 2 and 5) and r_e (20, 50, 100 and 130). Clouds at 200, 300 and 400 hPa have distinct ratios of 13, 18 and 32 (18, 35 and 87) for mid-latitudes (the tropics). It is obvious that the ratio increases depending on p_c , except for the polar region. Standard errors (σ/\sqrt{n}) are 8.0, 2.1 and near zero for the tropical, mid-latitude and polar atmospheric profile, respectively (error bars in figure 7). In all the profiled cases, the correlation coefficients (between $L_{10.8}^{cl} - L_{10.8}^{clr}$ and $L_{6.7}^{cl} - L_{6.7}^{clr}$) for the regression have nearly constant values between 0.82 and 1.00 (not shown). These high correlations indicate that clouds at a specific altitude have an inherent ratio regardless of their diverse τ_c and r_e . In general, a lower cloud in the tropics tends to have a smaller correlation value because water vapour in the atmosphere absorbs more 6.7- μm radiance from lower clouds.

The satellite zenith angle θ is also an important component to be considered for the calculation of $G_{6.7}^{10.8}$ in equation (5), while other angles such as θ and ϕ relative to the sun do not affect the 6.7- μm radiance. Table 4 shows the dependence of the ratios on various θ (0, 30 and 60) for mid-latitude winter. The ratio is greater for lower cloud regardless of θ . Here, all the ratios are calculated with a correlation coefficient of more than 0.93. It has also been found that a greater value of the ratio is computed for larger values of θ for the same p_c .

The choice of an appropriate clear-sky radiance is an important issue, as indicated in equation (5). The ratio from the measured radiance must be well matched with the pre-calculated ratio from the RT model in operational T_c and p_c retrievals. If the

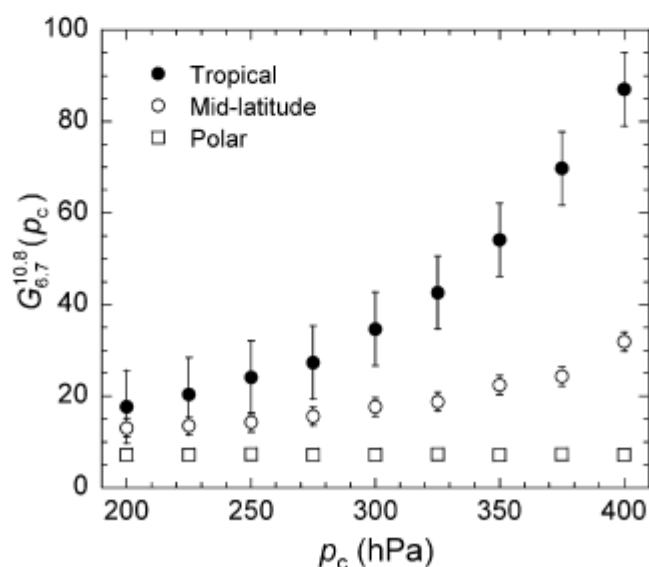


Figure 7. Simulation of radiance ratio ($G_{6.7}^{10.8}$) for single-layer ice clouds (at 200–400 hPa) under the condition of $\theta=30^\circ$ for the tropical (solid circles), mid-latitude (open circles), and polar atmospheric profiles (open squares). Values are plotted with standard errors (σ/\sqrt{n}).

Table 4. Ratios ($G_{6.7}^{10.8}$) calculated for various satellite scan angles (θ). This simulation was performed for clouds at 200, 300 and 400 hPa and for mid-latitude winter.

θ (deg)	200 hPa	300 hPa	400 hPa
60	16.2	23.0	48.5
30	13.1	17.7	31.9
0	12.4	16.6	28.9

ratio is calculated with improper clear-sky radiance for a cloudy FOV, it leads to serious uncertainty in T_c and p_c . COMS CLA takes up the method in which we find a maximum of clear-sky radiance between observed pixels adjacent to cloudy pixels in the $50 \text{ km} \times 50 \text{ km}$ FOV and simulated by the RT model with numerically predicted atmospheric profiles.

However, the MODIS current algorithm retrieves p_c by combining five ratios with MODIS CO₂ channels (G_{35}^{36} , G_{34}^{35} , G_{33}^{35} , G_{33}^{34} and G_{31}^{33}) after first estimates of the 10.8- μm radiance (Menzel *et al.* 2002). Here, G_{35}^{36} indicates the ratio using MODIS bands 36 and 35, in which the clear-sky radiance is obtained from the RT calculation with the aid of the National Centers for Environmental Prediction (www.cdc.noaa.gov). Therefore, the MODIS retrieval of p_c is accepted as the reference truth with an expected error of at least 50 hPa.

Figure 8 shows examples of the relationship between $G_{6.7}^{10.8}$ in the MODIS observation and the MODIS-retrieved p_c . $G_{6.7}^{10.8}$ values are simply calculated for each of the 5×5 pixels in the MODIS granules for 0155, 0200 and 0300 UTC of 4 March 2000, with the FOV covering Southeast Asia ($13^\circ\text{--}34^\circ \text{N}$, $113^\circ\text{--}150^\circ \text{E}$), the tropical western Pacific ($5^\circ \text{S}\text{--}16^\circ \text{N}$, $119^\circ\text{--}144^\circ \text{E}$) and Northeast Asia ($27^\circ\text{--}48^\circ \text{N}$, $100^\circ\text{--}132^\circ \text{E}$), respectively (box plots in figure 8). In the calculation of $G_{6.7}^{10.8}$, the clear-sky radiance is chosen as the maximum value among clear-sky pixels in 5×5 pixels, and the cloudy-sky radiance as the mean value of four cloudy pixels in 5×5 pixels. Accordingly, the 5×5 pixels in this calculation must include at least one observed clear-sky pixel, which prevents bias in our analysis that may be caused when using RT-simulated clear-sky radiance as a substitute for observed clear-sky radiance. The cases in 5×5 pixels, however, are not completely reliable as they hold only about 1% of the total in a granule. It is found that the distribution and median of values of $G_{6.7}^{10.8}$ increase with increasing p_c as a whole, although they show considerable ranges of the values (figure 8). These large ranges may arise because the calculation allows the conditions of θ of 0° to about 60° and of atmospheric profiles differing among pixels.

To compare the foregoing observational results with the RT calculation, $G_{6.7}^{10.8}$ is simulated by the Streamer in a manner similar to that shown in figure 7, but with the mean atmospheric profile in the granule under the conditions of 0° (solid circles) and 60° (open circles) in figure 8. Here, we used coincident retrieved atmospheric profiles with the ratio, which are provided in the MODIS atmospheric profile product (MOD07). This figure does not show the ratio induced by the regression analysis with correlation lower than 0.6 (clouds at lower than 325 hPa in figures 8(a) and 8(b)). The deviation between the MODIS observation and the RT calculation remains, as the atmospheric profile applied to the RT model is a mean value and may not be the exact truth (figures 8(a-c)). Water vapour contaminates the 6.7- μm radiance emitted from the cloud top below an altitude of 350 hPa even more than that from a higher cloud top in both the observation and RT calculation,

COMS cloud analysis algorithm

4729

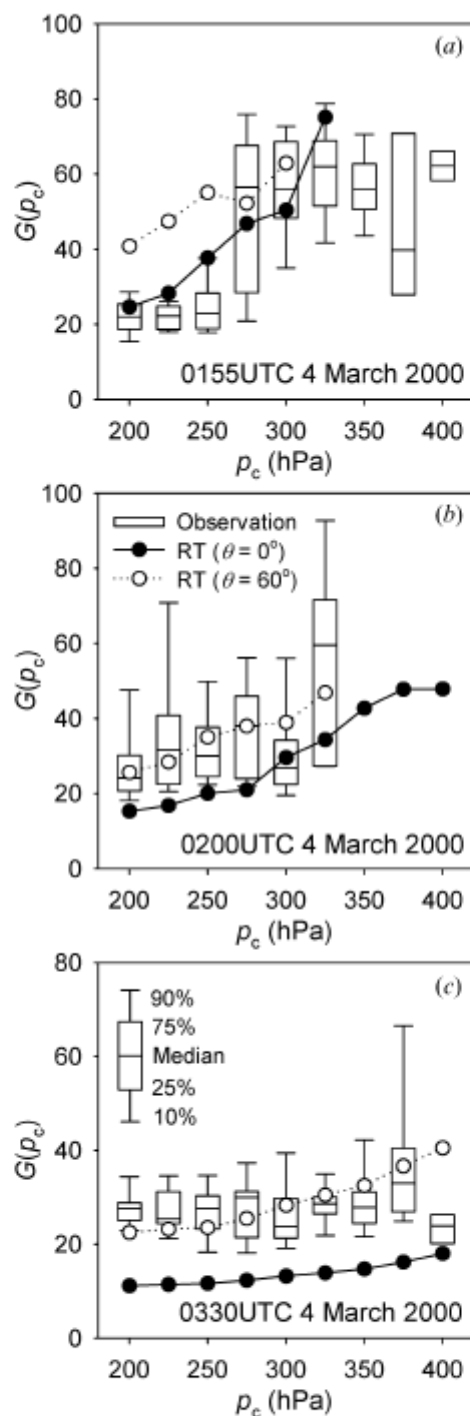


Figure 8. Box plot summing up the distribution, median and variability of radiance ratio ($G_{6.7}^{10.8}$) calculated from the MODIS granules for (a) 0155 UTC (13° – 34° N, 113° – 150° E), (b) 0200 UTC (5° S– 16° N, 119° – 144° E) and (c) 0330 UTC (27° – 48° N, 100° – 132° E) of 4 March 2000. The solid and open circles correspond to values of $G_{6.7}^{10.8}$ that are simulated by the RT model under the conditions of $\theta=0^\circ$ and 60° , respectively, for the mean atmospheric profiles over each of the granules.



국가기상위성센터
National Meteorological Satellite Center

Algorithm Theoretical Basis Document For Cloud Top Temperature and Pressure

Code:NMSC/SCI/ATBD/CTTP

Issue:1.0 Date:2012.12.26

File: CTTP-ATBD_V5.0.hwp

Page : 1/40

4730

Y.-S. Choi et al

particularly in the Tropics. Therefore, the observed $G_{6.7}^{10.8}$ and the RT result become ambiguous for clouds under 350 hPa (figures 8(a) and 8(b)). The large uncertainty for clouds under 350 hPa is relatively small in mid-latitude, but the derivative of the $G_{6.7}^{10.8}$ with respect to p_c is somewhat undersized (figure 8(c)). Consequently, the uncertainty seems to be inevitable in retrieving p_c by the ratio $G_{6.7}^{10.8}$ in at least 50 hPa, which corresponds to 3 K on average for inversed T_c .

6. Concluding remarks

The first Korean geostationary satellite, COMS, is scheduled to be launched in 2008. One of the most important meteorological mission objectives of COMS is to improve the prediction of severe weather events. The COMS Imager will have five channels at 0.6, 3.7, 6.7, 10.8 and 12.0 μm . This preliminary study suggests practical methods of retrieving cloud properties by fully utilizing the five channels of the COMS. The major characteristics of the methods are summarized as follows.

A new algorithm applying 6.7- μm in addition to 10.8- and 12.0- μm radiances has shown improved accuracy in the detection of the ice phase from the available data. This approach works comparatively well even in the absence of the 8.7- μm band, which is essential for the retrieval of the cloud phase in the MODIS IR trispectral algorithm.

The retrieval of τ_c and r_e using cloud-reflected 0.6- and 3.7- μm radiances is achieved by the rapid removal of undesirable radiance components. These components are obtained from a lookup table composed of angular variables, climatological A_g , and the 10.8- μm radiance measured for a coincident pixel. The τ_c (r_e) attained by this algorithm has shown a valid relationship, better below 20 (12 μm), than MODIS-retrieved τ_c (r_e) in its validation analysis using the available data.

The IR-window estimate using $BT_{10.8}$ was performed for the T_c and p_c of optically thick clouds ($\tau_c > 10$). The radiance ratioing method using 6.7- and 10.8- μm bands was introduced for optically thin high clouds (200–400 hPa). Contrary to the *in situ* methods using other sounding channels, it must consider two factors: θ and the atmospheric profile.

The limitations of the foregoing algorithm are the following. First, the ice phase can be overlooked for existing semitransparent clouds by this method of retrieval of the cloud phase. Thus, the method using $BT_{6.7}$ is efficient for most convective clouds. Second, the decoupling method slightly lowers the accuracy of τ_c and r_e . In particular, r_e can accumulate more noise by the additional removal of thermal components at 3.7- μm ($L_{3.7}^{\text{th}}$). As a result, the value of τ_c (r_e) over about 20 (12 μm) deviates more from the MODIS products. Third, the radiance ratioing method for T_c and p_c cannot be applied to clouds in polar regions. The performance of the method is relatively superior in the tropics, but clouds below 350 hPa are often contaminated by upper atmospheric moisture. The p_c estimated by this method presents a large bias compared with the MODIS-retrieved p_c . This bias may be lessened through an exact estimate of clear-sky radiance and an atmospheric profile.

Further studies remain to be performed on the validation of this method using MODIS data extended to other seasons. This should be carried out based on the conditions of abundant computer space and precise atmospheric profiles. There is also a need to perform a comparison of cloud products with similar data from other geostationary satellites and ground-based measurements collected at the Atmospheric Radiation Measurement Program. The influence of the lower



국가기상위성센터
National Meteorological Satellite Center

Algorithm Theoretical Basis Document For Cloud Top Temperature and Pressure

Code:NMSC/SCI/ATBD/CTTP

Issue:1.0 Date:2012.12.26

File: CTTP-ATBD_V5.0.hwp

Page : 1/40

COMS cloud analysis algorithm

4731

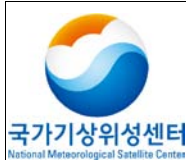
radiometric accuracy of COMS compared to the MODIS may debate the validity of the COMS CLA algorithm. Consequently, other geostationary satellites with five channels similar to COMS (e.g. MTSAT-1R) are expected to give us successful results for a prototype validation. The ground-based observation is usually limited to the cloud base, but its cloud optical properties will be useful in any future validation.

Acknowledgements

This study was undertaken for the COMS project funded by the Korean Meteorological Administration. Y.-S.C. and Y.-M.K. are supported by the BK21 project of the Korean government. We thank an anonymous reviewer for valuable comments. The MODIS data were provided by the Earth Observing System Data and Information System, Distributed Active Archive Center, at Goddard Space Flight Center, which archives, manages, and distributes these data.

References

- ACKERMAN, S.A., STRABALA, K.I., MENZEL, W.P., FREY, R.A., MOELLER, C.C. and GUMLEY, L.E., 1998, Discriminating clear-sky from clouds with MODIS. *Journal of Geophysical Research*, **103**, pp. 32141–32157.
- AHN, M.H., SEO, E.J., CHUNG, C.Y., SOHN, B.J., SUH, M.S. and OH, M., 2005, Introduction to the COMS meteorological data processing system. In *International Symposium on Remote Sensing*, 12–14 October 2005, Jeju, Korea (Seoul: The Korean Society of Remote Sensing), pp. 95–97.
- BAUM, B.A., SOULEN, P.F., STRABALA, K.I., KING, M.D., ACKERMAN, S.A., MENZEL, W.P. and YANG, P., 2000, Remote sensing of cloud properties using MODIS airborne simulator imagery during SUCCESS. 2. Cloud thermodynamic phase. *Journal of Geophysical Research*, **105**, pp. 11781–11792.
- CHOI, Y.S., HO, C.H. and SUI, C.H., 2005a, Different optical properties of high cloud in GMS and MODIS observations. *Geophysical Research Letters*, **32**, L23823, doi: 10.1029/2005GL024616.
- CHOI, Y.S., HO, C.H., AHN, M.H. and KIM, Y.S., 2005b, Enhancement of the consistency of MODIS thin cirrus with cloud phase by adding 1.6- μm reflectance. *International Journal of Remote Sensing*, **26**, pp. 4669–4680.
- CHOI, Y.S. and HO, C.H., 2006, Radiative effect of cirrus with different optical properties over the tropics in MODIS and CERES Observations. *Geophysical Research Letters*, **33**, L21811, doi: 10.1029/2006GL027403.
- ELLINGSON, R.G., ELLIS, J. and FELS, S., 1991, The intercomparison of radiation codes used in climate models: long wave results. *Journal of Geophysical Research*, **96**, pp. 8929–8953.
- HARTMANN, D.L. and MICHELSEN, M.L., 2002, No evidence for iris. *Bulletin of the American Meteorological Society*, **83**, pp. 249–254.
- KEY, J.R. and SCHWEIGER, A., 1998, Tools for atmospheric radiative transfer: Streamer and FluxNet. *Computers and Geosciences*, **24**, pp. 443–451.
- KEY, J.R. and INTRIERI, J.M., 2000, Cloud particle phase determination with the AVHRR. *Journal of Applied Meteorology*, **39**, pp. 1797–1804.
- KEY, J.R., 2002, *Streamer Version 3.0 User's Guide* (Madison, WI: NOAA/NESDIS). Available online at: stratus.ssec.wisc.edu.
- KING, M.D., 1987, Determination of the scaled optical thickness of clouds from reflected solar radiation measurements. *Journal of the Atmospheric Sciences*, **44**, pp. 1734–1751.
- KING, M.D., KAUFMAN, Y.J., MENZEL, W.P. and TANRE, D., 1992, Remote sensing of cloud, aerosol, and water vapor properties from the Moderate Resolution Imaging



Algorithm Theoretical Basis Document For Cloud Top Temperature and Pressure

Code:NMSC/SCI/ATBD/CTTP
Issue:1.0 Date:2012.12.26
File: CTTT-ATBD_V5.0.hwp
Page : 1/40

4732

COMS cloud analysis algorithm

- Spectrometer (MODIS). *IEEE Transactions on Geoscience and Remote Sensing*, **30**, pp. 2–27.
- KING, M.D., TSAY, S.C., PLATNICK, S.E., WANG, M. and LIU, K.N., 1997, Cloud retrieval algorithms for MODIS: optical thickness, effective particle radius, and thermodynamic phase. In *MODIS Algorithm Theoretical Basis Document* (NASA).
- LE GLEAU, H., 2005, *Software User Manual of the SAFNWC/MSG: Scientific Part for the PGE01-02-03. SAFNWC Software V1.2*. Available online at: <http://www.meteorologie.eu.org/safnwc/publis.htm>, pp. 35–53. Meteo, France.
- LINDZEN, R.S., CHOU, M.D. and HOU, A.Y., 2001, Does the earth have an adaptive infrared iris? *Bulletin of the American Meteorological Society*, **82**, pp. 417–432.
- MCCLATCHEY R.A., FENN, R.W., J. SELBY, E.A., VOLZ, F.E. and GARING, J.S., 1972, *Optical Properties of the Atmosphere*, 3rd edn. AFCRL Environment Research Paper No. 411, (Bedford, Massachusetts: Cambridge Research Laboratory), p. 108.
- MENZEL, W.P., SMITH, W.L. and STEWART, T.R., 1983, Improved cloud motion wind vector and altitude assignment using VAS. *Journal of Climate and Applied Meteorology*, **22**, pp. 377–384.
- MENZEL, W.P., BAUM, B.A., STRABALA, K.I. and FREY, R.A., 2002, Cloud top properties and cloud phase. In *MODIS Algorithm Theoretical Basis Document* (NASA), ATBD_MOD_04, NASA Goddard Space Flight Center. Available online at: http://modis-atmos.gsfc.nasa.gov/MOD06_L21.
- NAKAJIMA, T.Y. and KING, M.D., 1990, Determination of the optical thickness and effective particle radius of clouds from reflected solar radiation measurements, Part 1: Theory. *Journal of the Atmospheric Sciences*, **47**, pp. 1878–1893.
- NAKAJIMA, T.Y. and NAKAJIMA, T., 1995, Wide-area determination of cloud microphysical properties from NOAA AVHRR measurements for FIRE and ASTEX regions. *Journal of the Atmospheric Sciences*, **52**, pp. 4043–4059.
- OKADA, I., TAKAMURA, T., KAWAMOTO, K., INOUE, T., TAKAYABU, Y. and KIKUCHI, T., 2001, Cloud cover and optical thickness from GMS-5 image data. In *Proceedings GAME AAN/Radiation Workshop*, 8–10 March 2001, Phuket, Thailand (Nagoya: GAME International Project Office), pp. 9–11.
- PAVOLONIS, M.J. and HEIDINGER, A.K., 2004, Daytime cloud overlap detection from AVHRR and VIIRS. *Journal of Applied Meteorology*, **43**, pp. 762–778.
- RICCHIAZZI, P., YANG, S., GAUTIER, C. and SOWLE, D., 1998, SBDART: a research and teaching software tool for plane-parallel radiative transfer in the earth's atmosphere. *Bulletin of the American Meteorological Society*, **79**, pp. 2101–2114.
- SMITH, W.L. and PLATT, C.M., 1978, Comparison of satellite-deduced cloud heights with indications from radiosonde and ground-based laser measurements. *Journal of Applied Meteorology*, **17**, pp. 1796–1802.
- STRABALA, K.I., ACKERMAN, S.A. and MENZEL, W.P., 1994, Cloud properties inferred from 8–12- μm data. *Journal of Applied Meteorology*, **33**, pp. 212–229.
- TAKANO, Y. and LIU, K.N., 1989, Solar radiative transfer in cirrus clouds. Part I: Single scattering and optical properties of hexagonal ice crystals. *Journal of the Atmospheric Sciences*, **46**, pp. 3–19.
- WYLIE, D.P., MENZEL, W.P., WOOLF, H.M. and STRABALA, K.I., 1994, Four years of global cirrus cloud statistics using HIRS. *Journal of Climate*, **7**, pp. 1972–1986.